Modelling sea ice formation in the Terra Nova Bay polynya

Sansiviero M.[1], Morales Maqueda M. Á.[2], Fusco G.[1], Aulicino G.[1], Flocco D.[3] and Budillon G.[1]

[1] Università degli Studi di Napoli "Parthenope"

[2] School of Marine Science and Technology, Newcastle University (UK)

[3] Centre for Polar Observation and Modelling, University of Reading (UK)

Corresponding author: manusansi@inwind.it

Abstract

Antarctic sea ice is constantly exported from the shore by strong near surface winds opening leads and large polynyas in the pack ice. The latter, known as wind-driven polynyas, are responsible for significant water mass modifications due to the high salt flux into the ocean associated with enhanced ice growth. The Ross Sea is an oceanographic environment of interest being characterized by the presence of wind-driven polynyas. In particular we are going to focus on the Terra Nova Bay (TNB) polynya. Brine rejected during sea ice formation processes that occur in TBN polynya densifies the water column leading to the formation of the most characteristic water mass of the Ross Sea, the High Salinity Shelf Water (HSSW). This, in turn, takes part to the formation of the Antarctic Bottom Water (AABW), the densest water mass of the Southern Ocean which plays a major role in the global meridional overturning circulation affecting the global climate system. A coupled sea ice – ocean model has been developed to simulate the seasonal cycle of sea ice formation in, and export off, the polynya. The sea ice model accounts for both thermal and mechanical processes. The oceanic circulation is described by a reduced gravity model, one-and-a-half layer. The domain resolution is of 1 km, which is sufficient to represent the salient features of the coastline geometry, notably the Drygalski Ice Tongue. The model is forced by a combination of Era Interim reanalysis and in-situ data from automatic weather stations, and also by climatological oceanic dataset developed through in situ oceanic observations. The sensitivity of the polynya to the atmospheric forcing is well reproduced by the model when merging in situ and reanalysis data, which allows to capture in detail the strength and the spatial distribution of the katabatic winds. The model resolves accurately sea ice drift in TNB and sea ice production rates leading to realistic polynya extent estimates. The model-derived polynya extent has been validated. The comparison between the modelled sea ice concentration and the MODIS high resolution satellite images confirms that the model is able to reasonably reproduce the TNB polynya evolution in terms of both shape and numerical extent.

1. Introduction

Observations and models have clearly shown that changes in atmospheric forcing and ocean circulation affect the Antarctic sea ice extent (Jacobs and Comiso, 1997; Liu et al., 2004; Lefebvre et al., 2005; Zhang 2007; Turner et al., 2009; Liu and Curry, 2010). The strong pattern of increasing ice cover in the Ross Sea region, found to be the highest contributor among the five Southern Ocean sectors in 1979 - 2010 period with a positive trend of 13700 ± 1500 km^2 yr^{-1}, has been ascribed to changes in atmospheric circulation (Parkinson and Cavalieri, 2012). Enhanced northward winds have changed sea ice drift and export offshore affecting the dynamics of the local oceanography. These changes can impact the wind driven polynyas occurrence in Antarctic coastal areas modifying their activity and consequently the production of cold and salty water through sea ice growth processes (Holland and Kwok, 2012). Especially, variation in size or extent of polynyas are believed suitable indicators of climatic change (Morales Maqueda et al, 2004).

The wind-driven Terra Nova Bay (TNB) polynya, located in the western sector of the Ross Sea, plays a remarkable role in sea ice and ocean dynamics of this region (Kurtz and Bromwich, 1985; Bromwich, 1989). The polynya opening results principally from the synergy of meteorological and physical features of this region. Especially during the winter, TNB is frequently forced by cold and strong katabatic downslope flows that advect sea ice away from the coast. Their action prevents sea ice from consolidating as thick pack ice and at the same time allows its continuous formation leaving the relatively warm water ice exposed to the cold atmosphere. Also the presence and the orientation of the Drygalski Ice Tongue is essential for the polynya maintenance, since this barrier blocks the incoming sea ice from the south and controls through its length the polynya extent (Frezzotti and Mabin, 1994). Due to the constant formation and offshore drift of new ice, the TNB polynya contributes to sea ice mass budget of the whole area producing approximately 10% of sea ice annually formed in the Ross Sea (Kurtz and Bromwich, 1985; Van Woert, 1999b). Associated with the wind-forced ice production is a salt flux that causes haline convection affecting the characteristics of the entire water column at TNB and the thermohaline structure of the whole Ross

Sea (Kurtz and Bromwich, 1985; Trumbore et al., 1991). TNB polynya is considered to be by far the largest producer of High Salinity Shelf Water (HSSW) (Kurtz and Bromwich, 1983, 1985; Jacobs et al., 1985; Van Woert, 1999a, b; Budillon and Spezie, 2000; Budillon et al., 2003; Fusco et al., 2009) that plays a crucial role in the formation of Antarctic Bottom Water (AABW) (Kurtz and Bromwich, 1985; Jacobs and Comiso, 1989; Van Woert, 1999a), contributing significantly to the deep ocean ventilation and the global thermohaline circulation (Jacobs et al., 1985; Orsi et al., 1999; Jacobs 2004).

The main goal of this study is to investigate the sea ice behaviour in the Terra Nova Bay polynya in response to external forcing and to estimate the associated sea ice and HSSW production. To this purpose a coupled sea ice – ocean model was developed and applied to Terra Nova Bay. The model simulates the seasonal cycle of sea ice formation in Terra Nova Bay polynya accounting for both sea ice dynamic and thermodynamic processes. The first ones produce no ice directly, but cause the ice drifting (horizontal transport) in or off the area and its deformation as a result of rafting, ridging and convergence/divergence phenomena. On the contrary, the latter are responsible for local ice growth or melt and heat transfer between the involved surfaces (Rothrock, 1979). Both kind of processes alter the local mean thickness (ice volume per unit area) and involve exchanges of mass (fresh water) and energy with the atmosphere and ocean (Flato, 2003).

A further target of this work is the estimate of the TNB polynya extent, characterized by areas with low sea ice concentration. Computing the polynya extent is a hard matter depending on the accuracy and the limitations of the models and the remote sensing tools, as well as on their capability to resolve in time and in space the processes involved in the polynya variability. Polynya extent estimates are not trivial to retrieve since local ice thickness or ice production rates are often unknown. Papers focusing on the variability of sea ice and open water concentration in TNB exist in literature, mainly concerning the wintertime season. Some authors investigated the polynya extent through one dimensional models forced by in situ and reanalysis data (Van Woert, 1999a, 1999b; Fusco et al., 2002; Petrelli et al., 2008) or through satellite observations (Kern, 2007; Ciappa et al., 2012). The polynya extent here is retrieved from sea ice concentration and validated by the comparison with polynya extent detected from MODIS satellite images.

The paper is organized as it follows. Section 2 provides a description of the coupled sea ice – ocean model and the main formulations adopted to resolve sea ice dynamics and thermodynamics. Section 3 presents some sensitivity experiments with respect to specific physical factors and parameterizations in order to tune the model to the peculiarities of TNB region. In particular, sea ice behaviour in the polynya area in response to the wind forcing is highlighted. Section 4 shows the results of one year simulation of sea ice formation in TNB region as well as the polynya extent estimates. Section 5 focuses on the comparison between the TNB polynya extent estimates and the high resolution MODIS images. Finally, discussion and concluding remarks are outlined in Section 6.

2. Description of the model

The coupled sea ice – ocean model presented here is a simple general circulation model (GCM) applied to the TNB polynya. In contrast with the polynya flux models describing the evolution of a polynya in terms of the polynya edge contour, it predicts sea ice concentration as distributed over some regular spatial grid within a given domain (Wilmott et al., 2007). The model is run at high resolution (1 km) in order to cope with the complexity of the coastline geometry and the meteorological patterns of this region. Both dynamic and thermodynamic processes of sea ice are incorporated in the model. An accurate representation of the main sea ice processes, often overlooked in numerical simulations of the polar regions (Russell et al., 2006; Maksym et al., 2012) and, a realistic sea ice dynamics, especially in the Southern Ocean, are crucial to describe the interaction of thin ice and polynyas with the atmospheric and oceanic circulation (Stössel et al, 1990). The ocean is represented by a one-and-a-half layer reduced gravity ocean model in which the oceanic dynamics satisfy the hydrostatic equilibrium and the Boussinesq approximation. Then, the stratification is simplified as a two-layer fluid in which the active layer (mixed layer) moves above a lower stagnant (motionless) layer of infinite depth. Sea ice behaves as a floating zero layer system without thermal inertia, as proposed by Semtner (1976), interacting thermodynamically with the atmosphere and the underlying mixed layer of the ocean. The coupling of sea ice with the surface ocean layer allows us to simulate the seasonal cycle of sea ice formation in, and export off the polynya. The model requires atmospheric and ocean forcing as inputs that are applied as surface and bottom boundary conditions. The atmospheric forcing is given by air temperature, surface pressure, humidity, cloud cover, precipitation and wind fields. The model needs also the solar radiation in order to compute the balance of radiative and the turbulent heat fluxes. The ocean forcing consists of the ocean temperature and salinity profiles. The main variables involved in the coupled sea ice-ocean model are shown in Fig.1 as well as the heat balance at air-ocean, air-ice and ice-ocean interfaces.

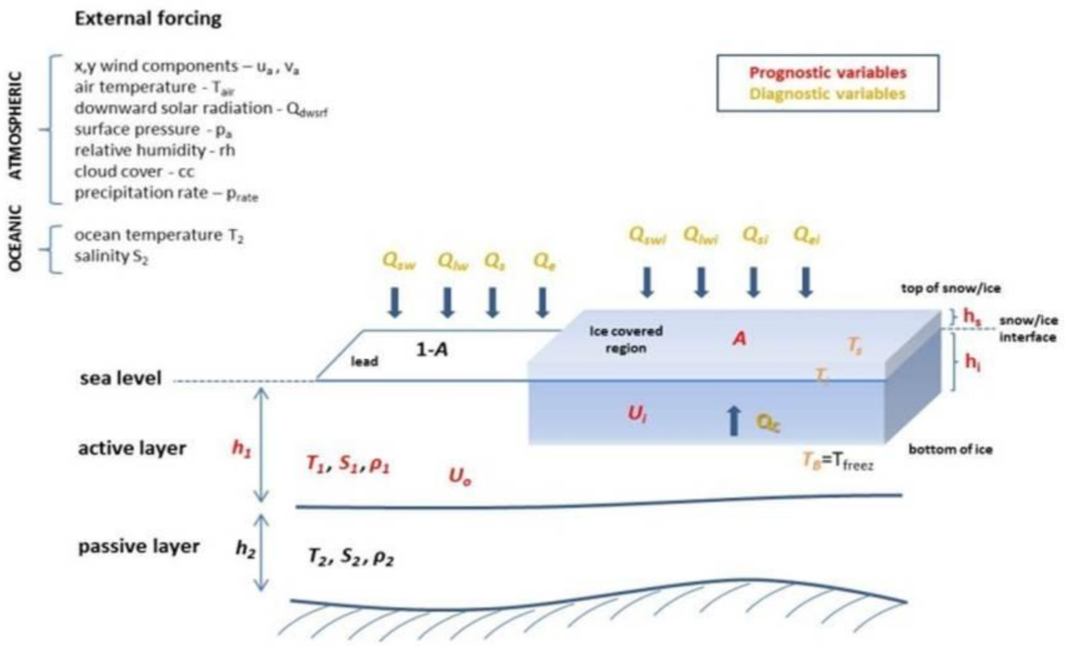

Fig. 1: Schematic view of the main variables of the coupled sea ice – ocean model. The radiative and turbulent heat fluxes (Wm^{-2}) are separately calculated over the ice free (leads) and ice covered part of a grid cell. The positive vertical direction is downward.

Sea ice is characterized by the ice concentration (A), defined as the fraction of a grid cell covered by ice varying between zero and one and by the ice thickness (h_i). The non-covered fraction of each grid cell (1-A) is referred to as a lead. Sea ice is allowed to be covered by a snow layer (h_s) that is important for the determination of the growth rates of sea ice (Stössel et al., 1990). Also, snow-ice formation from Fichefet and Maqueda (1999) which takes part in the thickening of sea ice is prescribed. A, h_i and h_s are prognostically calculated by continuity equations including dynamic and thermodynamic terms. Sea ice drift, that is the ice velocity $\mathbf{U_i}$ (u_i, v_i) is computed by the momentum equation expressed as the force balance among the Coriolis force, wind and ocean stresses and interaction between floes due to ice deformation. The atmosphere and ocean stresses parameterization includes the ice concentration as a multiplicative factor to be consistent with the theory of free drift in regions of low ice concentration according Connolley et al. (2004). The internal ice forces are resolved using the elastic-viscous-plastic rheology by Hunke and Dukowicz (1997), where the coupling between the dynamics and sea ice thickness (h_i) and concentration (A) is allowed through the internal ice pressure (see more in section 3.1) as in Hibler's (1979) formulation. The active layer of the ocean is maintained at the freezing point as long as ice is present. It is simply represented by one layer of a depth h_1, temperature T_1, salinity S_1 and density ρ_1, the latter from Maqueda et al. (1999), which are determined by the entrainment of water from the motionless infinitely deep layer (h_2) of a prescribed temperature T_2, salinity S_2 and ρ_2. The entrainment velocity depending on air-sea fluxes that control the strength of turbulence in the mixed layer is described following the Lemke (1987) parameterization. The oceanic variables together with the ocean velocity, $\mathbf{U_o}$ (u_o,v_o) are calculated prognostically via continuity and momentum equations as for the ice. The stress term is from Mellor and Kantha (1989) and is described by the combination of the shear stress at the surface of ice covered ocean and the wind stress acting at the surface of ice free ocean. The vertical turbulent mixing and dissipation due to the bottom friction at the base of the active layer is prescribed according to the parameterization of Pacanowski and Philander (1981). The radiative and the turbulent heat fluxes are calculated separately following

Budillon et al. (2000) over the leads (Q_{sw}, Q_{lw}, Q_s and Q_e) and the ice covered parts (Q_{swi}, Q_{lwi}, Q_{si} and Q_{ei}). The conductive heat flux (Q_C) through the ice contributes to the net heat balance determining the thermodynamic changes in ice thickness and concentration due to vertical and lateral processes. In computing sea ice production, the temperature at the base of ice T_B is set at the freezing point and the ice surface temperature T_s and the temperature at snow-ice interface T_i are calculated diagnostically from this balance.

2.2 Model domain and set up

The model domain consists in a wide region of the western Ross Sea including an extended area along the coast of Victoria Land south of the Drygalski Ice Tongue and the northern region of the Wood Bay. It is 488 km long and 154 km large extending approximately from 74°S to 78°S in latitude and from 162°E to 168°E in longitude. A spatially uniform horizontal resolution of 1 km is used to study the small scale behaviour of sea ice in TNB. It is also considered to be sufficient in representing the salient features of the coastline geometry such as the Drygalski Ice Tongue. Hence the horizontal grid is a rectangle of XY dimensions subdivided in square grid cells resulting in a grid of 154 × 488 = 75152 grid points. The Arakawa B-grid is used for the spatial discretization where all the scalar variables, such as the thermodynamic and transport variables are computed at the center of the grid cell, while all the vector variables are defined at the corners. Hence two masks have been created for these two sets of variables. A land mask is specified in the center of the cells with 0 representing land and 1 oceanic cells. A corresponding mask is defined for all corner quantities such as the wind speed, sea ice velocity and stress components. The advection equation is discretized with a first order upstream scheme. The solutions of the momentum equations and the advective and thermodynamic processes are computed using two different time steps: a small one for the momentum (Δt) and a larger one for the advection (ΔT_a). All the input parameters such as constants and coefficients are shown in Table 1. The x stands for a varying value in the performed experiments. Sea ice concentration and thickness and ocean fields are initialized at the beginning of each integration with a prescribed value or with a restart from the previous integration.

Open lateral boundary conditions ensuring a minimum of signal reflections at the boundary have been used so that advective flows leaving the domain are allowed to freely exit the domain using an upstream formulation, while flows into the domain use a simple sponge boundary condition that relaxes the variables to their climatological external values (Martinsen and Engedahl, 1987). The main physical parameters of atmosphere, sea ice and ocean used in the model are showed in Table 2.

Parameter	**Symbol**	**Value**
X domain	X	154000 m
Y domain	Y	488000 m
T domain	T	x^* days
Time step for momentum	Δt	600 s
Time step for advection	Δta	1.2 s
Elastic timescale	Δte	180 s
Air drag coefficient	C_{da}	x^*
Ocean drag coefficient	C_{do}	x^*
Ice strength parameter	P^*	x^* N/m^2
Ice concentration parameter	C	20
Creep limit	c	5×10^{-11} 1/s
Eccentricity of the elliptical yield curve	e	2
Demarcation ice thickness	h_{pu}	x^* m

Table 1: Input parameters of the model.

Parameter	**Symbol**	**Value**
Thermal conductivity of sea ice	κi	2.2 W/m/K
Thermal conductivity of snow	κ_s	0.3 W/m/K
Emissivity of atmosphere	ε_a	0.95
Emissivity of ocean	ε_o	0.985
Albedo of ocean	α_o	0.07
Albedo of ice	α_i	0.07-0.7
Albedo of snow	α_{sn}	0.85
Latent heat of fusion of ice	L_{fi}	3.34×10^5 J/m^3
Latent heat of vaporization of water	L_e	2.5×10^9 J/m^3
Latent heat of fusion of snow	L_{fsn}	3.34×10^5 J/m^3
Latent heat of sublimation of snow	L_{ssn}	2.834×10^6 J/m^3
Specific heat capacity of ocean	c_{pa}	3985 J/m^3/°C
Specific heat capacity of air	c_{po}	1004 J/m^3/°C
Density of air	ρ_a	1.3 Kg/m^3
Density of ice	ρ_i	900 Kg/m^3
Density of snow	ρ_s	330 Kg/m^3
Density of ocean	ρ_o	1024 Kg/m^3
Melting point of freshwater ice	t_{fus}	0°C
Salinity of sea ice	s_i	4 psu
Exchange coeff. for sensible heat (leads/ice)	c_H	1.75×10^{-3}
Exchange coeff. for latent heat over leads	c_E	1.75×10^{-3}
Exchange coeff. for latent heat over ice	c_E	1×10^{-3}
Stefan-Boltzmann constant	K	5.67×10^{-8}
Minimum vertical viscosity	υ_{min}	1×10^{-3}

Table 2: Physical parameters of atmosphere, sea ice and ocean.

Fig. 2 outlines the diagram flow of the coupled sea ice-ocean showing the basic steps in computing the diagnostic variables of the model.

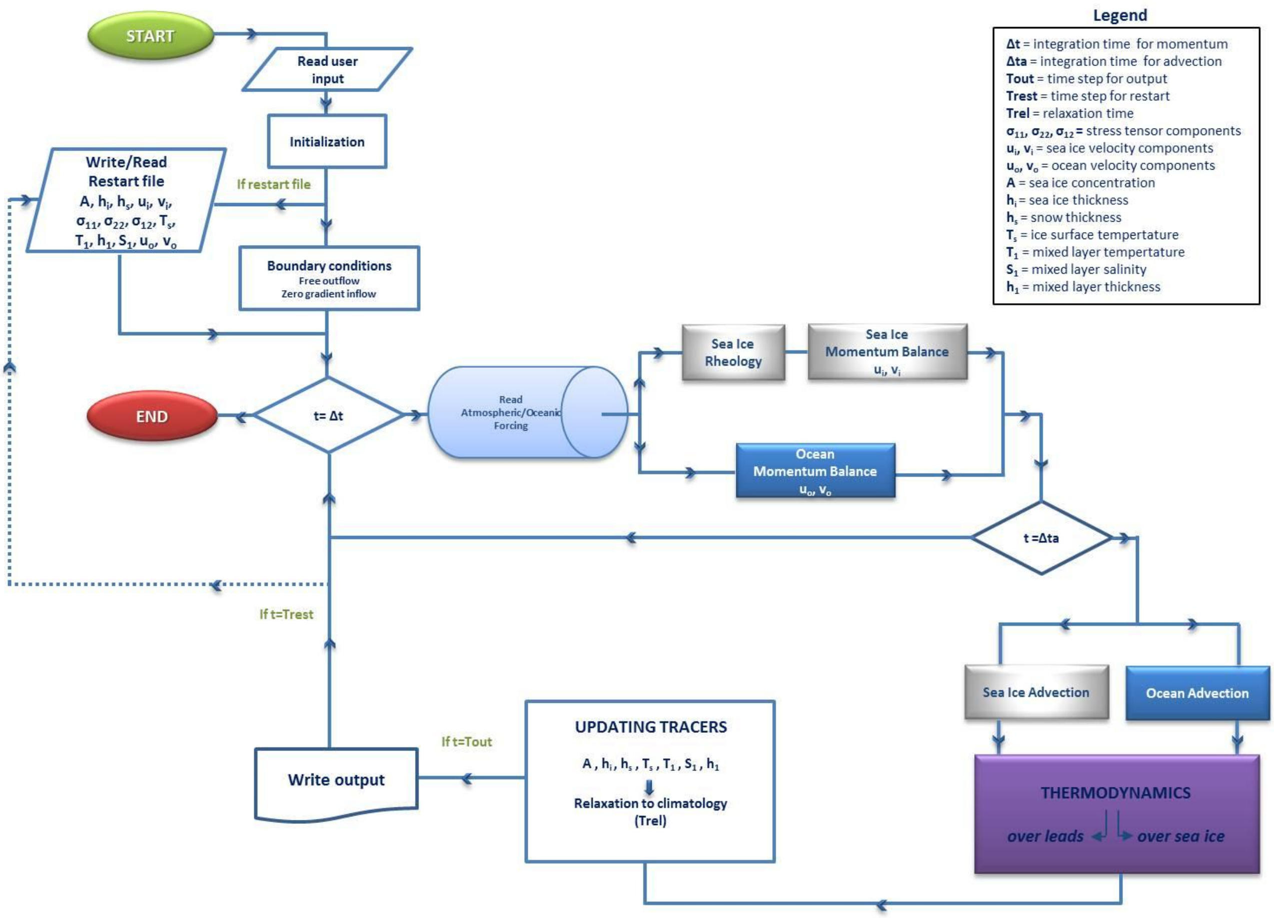

Fig. 2: Diagram flow of the coupled sea ice-ocean model.

2.2 Forcing fields

The ocean forcing consists of climatological oceanographic profiles of ocean temperature and salinity developed through the analysis of available in situ temperature and salinity datasets. These datasets consist of hydrographic mooring and CTD profile data collected from February 1995 to January 2008 within the CLIMA (Climatic Long-term Interaction for the Mass-balance in Antarctica) project of the Italian National Research Antarctic Program (PNRA). The two climatological datasets include idealized monthly temperature and salinity values, spatially uniform in the model domain and varying vertically up to 800 meters in depth. In detail, 8 depth levels (0 m, -30 m, -50 m, -100 m, -150 m, -300 m, -500 m, -800 m) are chosen for the computation of the oceanic mixed layer, so that the temperature and salinity profiles consist of 8 monthly values. As main atmospheric forcing, the Era-Interim reanalysis from the European Centre for Medium-Range Weather Forecasts (ECMWF), has been prescribed. The data extracted from the global domain provide surface six-hourly parameters at a 0.5 × 0.5 degree horizontal resolution covering the model domain with 16x11 grid points, in latitude and in longitude respectively. Specifically, the input data consist of the 10 meter eastward and northward wind components (m/s), the 2 meter temperature (K), the downward surface solar radiation ($Wm^{-2}s$), the surface (1000 mb level) pressure (Pa), the relative humidity (%), the total cloud cover (0-1) and the precipitation rate (m of water). The oceanographic and atmospheric data have been spatially and temporally interpolated over the whole model domain. Meteorological observations form Automatic Weather Stations (AWSs) have been also employed to force the model.

2.2.1 Atmospheric field setting

The resolution of the local winds is a crucial factor in estimating sea ice production especially in a small coastal polynya like the TNB one. In particular during winter, sea ice production in TNB is largely determined by katabatic winds which are the main forcing of the TNB polynya size (Petrelli et al., 2008; Gallé, 1997). Petrelli et al. (2008) showed that a simplified resolution of the katabatic winds leads to an underestimation of sea ice winter production of up to 50% which results in an underestimation of the formation rate of HSSW and consequently of AABW. In spite of their relatively high resolution, the ECMWF reanalysis have been found to underestimate the wind speeds in several studies (Cullather et al., 1997; Fusco et al., 2002; Petrelli et al., 2008) providing therefore an improper representation of the wind fields along and offshore TNB. A wind correction has been applied to coastal and offshore model grid points value combining the Era Interim data with in-situ atmospheric data from Automatic Weather Stations (AWSs) which show a significantly increased skill over ECMWF atmospheric variables (Petrelli et al., 2008).

A merging function has been designed so that the correction factor for each grid point value varies with the distance from the weather station. Era Interim and AWS data are merged resulting in the effective wind vector defined as

$$V_{eff} = V_{AWS}\, e^{-\frac{r}{R}} + V_{Era}\left(1 - e^{-\frac{r}{R}}\right)$$

where V_{AWS} and V_{Era} are the wind vectors from AWS and ERA-Interim respectively, r is the distance from the AWS and R is an e-folding length scale so that the influence range of the AWS depicts a circumference.

In particular, atmospheric data from two AWSs have been used. In a first phase of the sensitivity tests only Rita AWS (-74.72° S, 164.03° E), installed within the Meteo-Climatological Observatory of the PNRA in proximity of the Italian base “Mario Zucchelli” downstream of the Priestley Glacier, has been considered.

Successively, Manuela AWS (-74.95° S, 163.69° E), installed within the AWS project of the University of Wisconsin-Madison Antarctic Meteorology Program on Inexpressible Island has been also included. The AWS Manuela lies downstream of the Reeves Glacier which represents the main area of confluence of the katabatic flows from the interior of Antarctica.

Rita e Manuela datasets consist, respectively, of one hourly and ten minute intervals data relative to air temperature (°C), wind speed (m/s) and direction, surface pressure (hPa), relative humidity (%). The merging function has been applied also for the air temperature and relative humidity data.

3 Sensitivity experiments

An improper choice of the parameters which describe sea ice evolution results often in unrealistic simulations leading to inaccurate results of sea ice outputs. Several sensitivity experiments were performed to define the best set of parameters controlling TNB sea ice dynamics and thermodynamics in response to wind forcing. Two key parameters have been found to control the wind driven polynyas: the rheology ice strength parameter P^* and the demarcation ice thickness H, named also lead–closing parameter, that is simply the prescribed thickness of new ice formed in leads. The rate at which the leads close under freezing conditions is inversely proportional to the value of H. Both parameters have a strong effect on polynya size and sea ice extent and volume estimates (Hibler, 1979; Stössel et al., 1990; Stössel, 1992).

Finally a sensitivity analysis was carried out turning attention to the air-ice and ice-ocean drag coefficients which control the wind stress on the sea surface and sea ice. The choice of these parameters depends on the study area and especially on the wind forcing time and spatial resolution, therefore the model was opportunely tuned and optimized with respect to them.

3.1 Sensitivity to ice strength parameter

The ice strength parameter $P*$ is a key element in sea ice rheology that relates sea ice strength (P) to its concentration (A) and mean thickness (h). It was first introduced by Hibler (1979) in the constitutive equation for sea ice strength as

$$\mathrm{P} = P^{*}\mathrm{he}^{[-\mathrm{C}^{*}(1-\mathrm{A})]}$$

where $P*$ and C* are empirical values. Ice strength exhibits a strong dependence on sea ice concentration and especially on the amount of the thin ice/open water $(1 - \mathrm{A})$. For low ice concentrations the ice strength decreases significantly and most of the sea ice is deformed (Hibler, 1979; Wilmott et al., 2007, Feltham, 2008). Sea ice also offers less resistance to compression when h and $P*$ are low, and tends to pile up more easily because of enhanced mechanical ridging and rafting. Then, $P*$ is a critical parameter controlling sea ice drift behaviour in the wind driven polynyas and, therefore, it represents the main tuning parameter to achieve a realistic sea ice drift pattern (Owens and Lemke, 1990; Stössel et al., 1990; Steele et al., 1997).

Some experiments have been carried out to observe the impact of $P*$ on sea ice dynamics in TNB. Also the influence of the merging function and the size of the R factor on sea ice evolution have been considered. Table 3 displays the different combination of $P*$ and the merging conditions varying alternately in these experiments. The control experiment referred to as CASE 1 run using a $P* = 27500 \times 10^4$ N/m^2 by Hibler and Walsh (1982) that is the most widely used value for the ice strength parameter and R=25 km. The CASE 2 is different from the control run just for $P* = 5000$ N/m^2 as in Hibler (1979), while the CASE 3 and CASE 4 differ from the control experiment in the absence of the merging between reanalysis and AWS data and in the larger influence range of AWS data respectively.

Experiment	P^* (N/m^2)	R factor (km)
CASE 1	*27500*	*25*
CASE 2	*5000*	*25*
CASE 3	*27500*	-
CASE 4	27500	*50*

Table3: Sensitivity tests of sea ice evolution with respect to P^* and R factor.

In all the runs the demarcation ice thickness - H was set to 0.1 m. Regarding the oceanic forcing, a relaxation time of 7 days to climatological data was set in all the experiments. The time interval of the atmospheric input was set to 6 hours, while that of the output fields to 1 day so that the model gives a daily output for each computed variable. Fig. 3 (a, b) depicts the wind forcing and the respective ice drift fields on 8th July 2000. The CASE 1 and the CASE 2 exhibit the same wind fields being forced with the same wind configuration. The wind velocities present maximum values of 19.66 m/s in CASE 1/CASE 2 and 20.65 m/s in CASE 4, while in CASE 3, where the merging function is switched off, they reach a maximum value of only 7.27 m/s. The mean and minimum values are 6.03 m/s and 4.67 m/s for the CASE 1/CASE 2, 8.03 m/s and 6.19 m/s for CASE 4 and 5.68 m/s and 3.18 m/s for CASE 3. The ice velocities show max values of 0.32-0.34 m/s and mean values of 0.05-0.08 except in CASE 3, where the ice drift is forced only by the ERA-Interim data, showing smaller max and mean values of 0.1 m/s and 0.03 m/s respectively.

It can be observed that for large wind and ice velocities the polynya responds with large extents (CASE 1) even though sea ice concentration and thickness distributions resulting from the CASE 2, CASE 3 and CASE 4 are very similar to those simulated by the control experiment. The reduced ice strength does not affect significantly the ridging of sea ice as well as sea ice drift in convergent regions altering relatively little the ice concentration and thickness distribution. This indicates the polynya area is not highly sensitive to P^* in the determination of its opening/closure for this set of forcing. This is probably due to the major influence of this parameter in areas of thick ice rather than in region formed by thin and broken ice cover (Kreysher et al., 2000). On the contrary an increasing of R factor (Case 4) leads, as expected, to larger ice drift velocities and hence to a greater polynya opening.

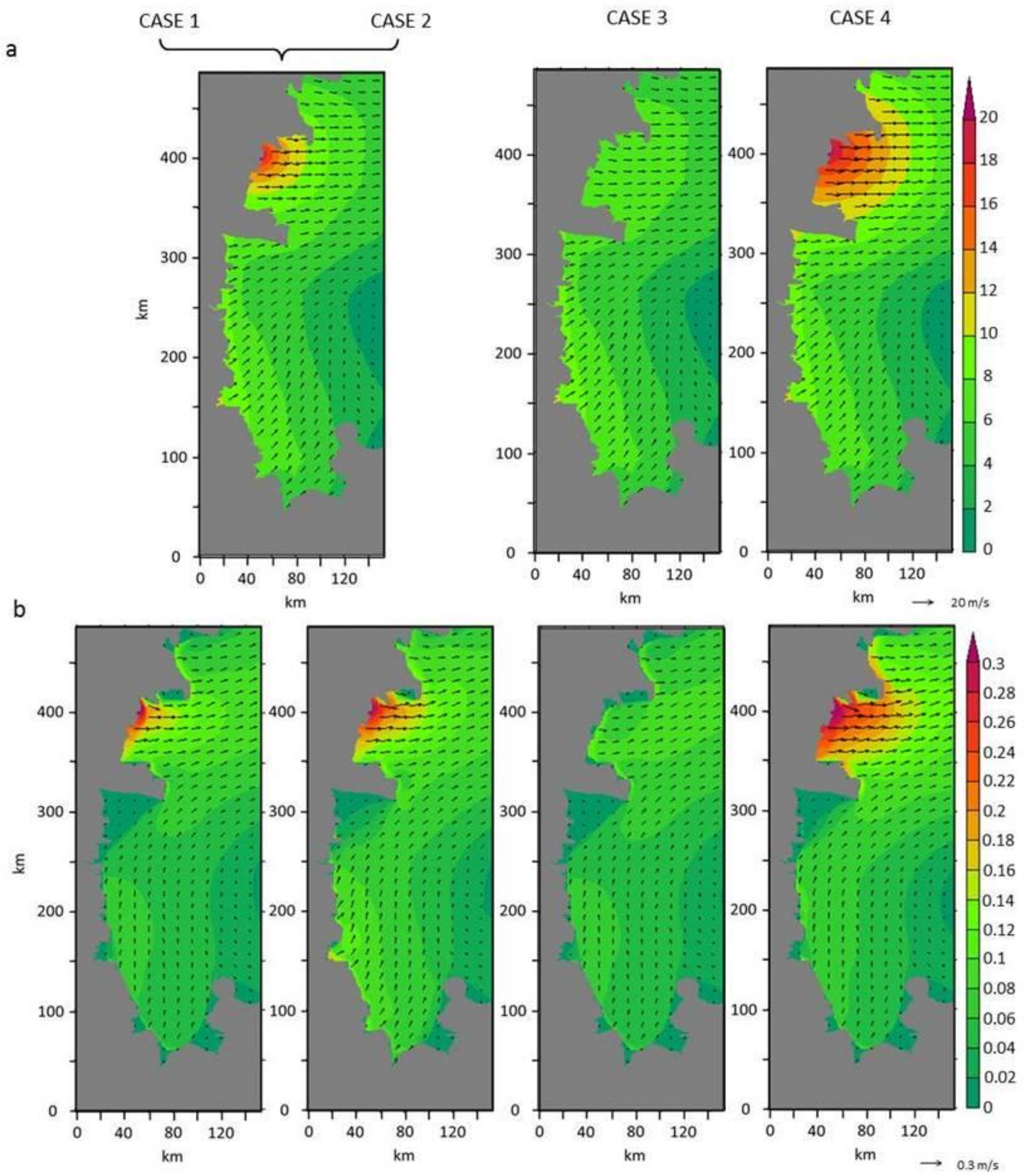

Fig. 3: Maps of wind velocities (a) and modelled ice drift velocities (b) on 8th July 2000 for CASE 1/CASE 2, CASE 3 and CASE 4.

2.2 Sensitivity to demarcation ice thickness

While the behaviour of the consolidated ice is mostly determined by the ice rheology, the interior of the polynya is affected by the new ice thickness parameterization. The new ice thickness is controlled by the demarcation ice thickness parameter H (Hibler, 1979) that is expressed as a transition value between thin ice (open water) and thick ice. It is a crucial element in sea ice models as the ice thickness collection depth in polynya flux models, since it represents the thickness at which newly-formed ice in the polynya is transferred into thicker solid sea ice. Thereby it affects sea ice thermodynamics lowering heat loss through thin ice inside the polynya and determining primarily the mean thickness and sea ice concentration (Hibler, 1979; Olason and Harms, 2010).

H has been often defined constant in literature assuming a value in the range 0.1-0.5 m (Hibler, 1979; Pease, 1987; Ou, 1988; Darby et al. 1994, 1995). However the wind speed is considered to be an important part of the new ice thickness parameterization (Mellor and Kantha, 1989; Winsor and Björk, 2000; Olason and Harms, 2010).

Few experiments showed in Table 4 were performed with different values of *H*. The control experiment (CASE 5) was run with *H*=0.2 m, that is considered more appropriate than the 0.5 m proposed by Hibler (1979) in simulating the behaviour of the thin ice inside the polynya (Olason and Harms, 2010). In the second (CASE 6) and third experiment (CASE 7) sea ice concentration and thickness are simulated using a constant *H*=0.3 m and *H*=0.4 m respectively, while in the fourth one (CASE 8) a varying *H* has been used. In particular the collection depth parameterization of Winsor & Björk (2000) is employed assuming the demarcation thickness to be a function of the wind speed:

$$H = \frac{a + |V| \cdot b}{c}$$

where V is the surface wind velocity and the constants are a = 1, b = 0.1 and c = 15. That means that *H* varies in the range 0.1-0.3 m in presence of wind speeds between 5-35 m/s.

In all the experiments R is fixed to 50 km except in CASE 9 in which the merging function is not applied. The value of 27500 N/m^2 for P* and of 30 days for the relaxation time to oceanic forcing have been used. Fig. 4 shows the results of sea ice concentration and thickness simulation on 8th July 2000 for the CASE 5 - CASE 9. Note that a lower ice demarcation thickness value gives higher ice concentration values and lower ice thickness values resulting from enhanced heat losses over open water and thin ice especially during winter (Maykut, 1978).

Experiment	*H* (m)	R factor (km)
CASE 5	0.2	50
CASE 6	0.3	50
CASE 7	0.4	50
CASE 8	f (V)	50
CASE 9	0.2	-

Table 4: Sensitivity tests of sea ice evolution with respect to H and R factor.

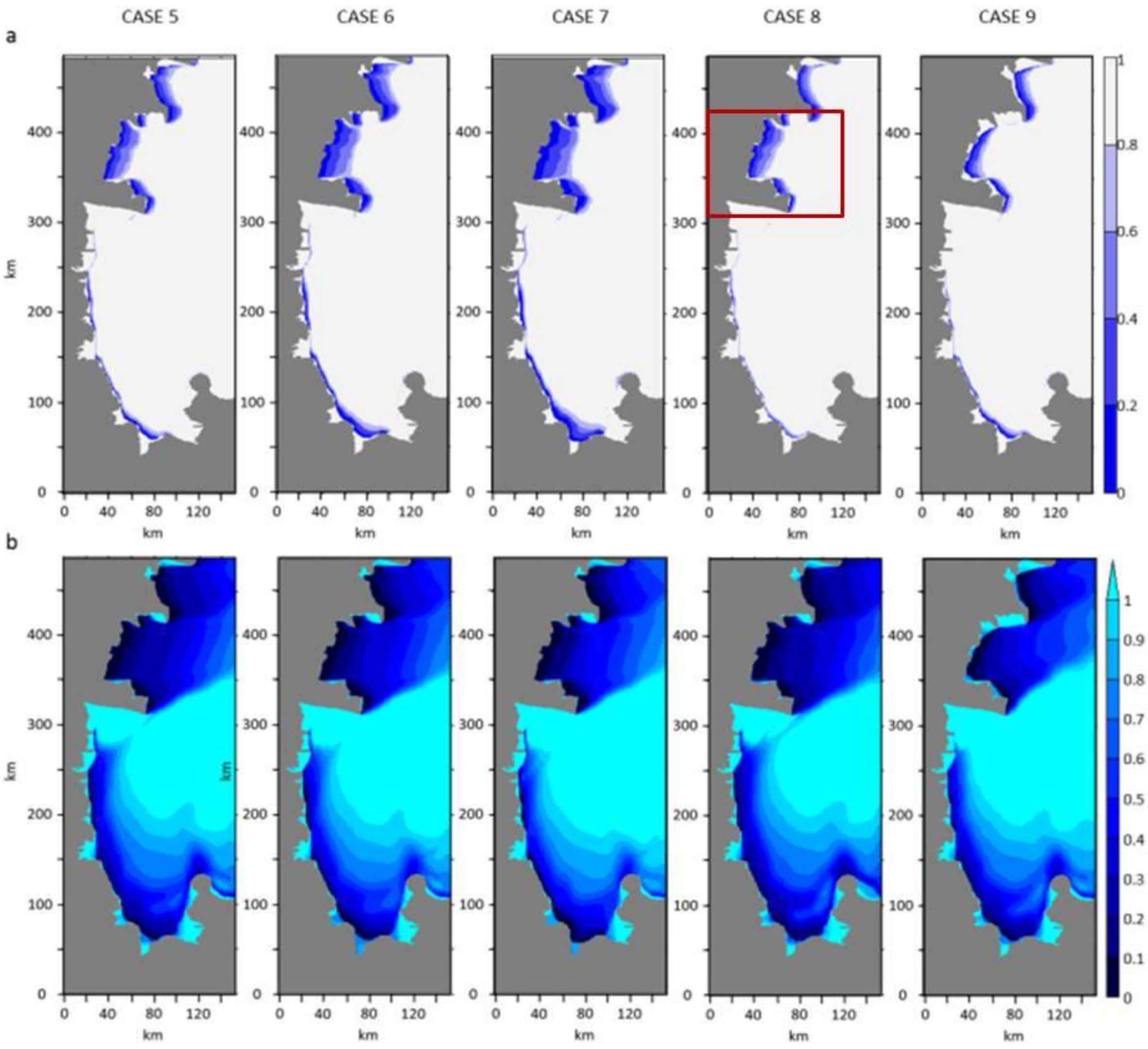

Fig. 4: Simulation maps of sea ice concentration (a) and sea ice thickness (b) for CASE 5, CASE 6, CASE 7, CASE 8 and CASE 9 on 8th July 2000. The portion of the domain marked by the red box in (a) is the area defined for computational purposes as TNB region extending approximately from 310 km to 425 km in Y and bordered by X = 120 km .

The CASE 8 results are similar to the sea ice distribution observed in CASE 5 suggesting that the dependence of sea ice evolution on the wind velocities provides plausible values for *H*. This is well supported by the estimates of daily sea ice production (km^3/day) in TNB area on July 2000 (Fig. 5) derived from sea ice concentration fields for all the experiments. Cumulative sea ice production (km^3) for the whole of July 2000 is also showed in Table 5. Note that the TNB area is identified by the region of the domain that extends within the ranges 1-120 km in X (longitude) and 310-425 km in Y (latitude) as shown in Fig. 4. Sea ice production rate computed using a non-spatially uniform *H* (CASE 8) depicted by the magenta line shows a trend very similar to that of the CASE 1 except for a few days when it exhibits larger wind velocities. As it can easily be observed, CASE 9, where wind forcing is given by the winds reanalysis alone, underestimates considerably sea ice production rate compared to the CASE 5 and all the others. The results suggest that the model reproduces quite well the relationship between the wind forcing and sea ice dynamics in TNB and the modelled variables are fairly realistic.

However, more satisfying simulations of sea ice output fields can be achieved investigating more extensively the wind forcing (Stössel et al. 2011) and the resulting wind stress in the TNB causing the increasing or decreasing of the open water and thin ice extent.

Experiment	**Sea Ice production (km^3) in July 2000**
CASE 5	10.08
CASE 6	11.09
CASE 7	12.12
CASE 8	9.79
CASE 9	6.83

Table 5: Sea ice production in July 2000 for the CASE 5, CASE 6, CASE 7, CASE 8 and CASE 9 experiments.

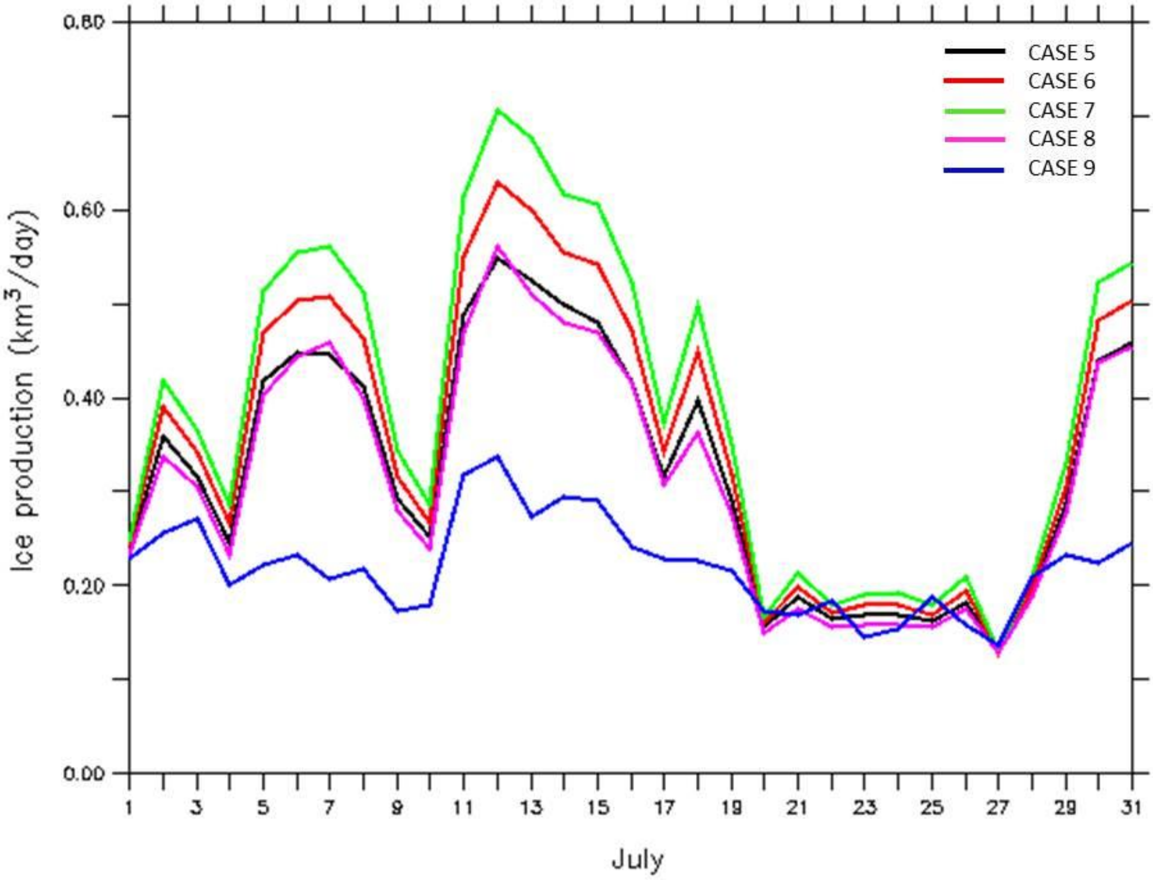

Fig. 5: Daily ice production in the TNB region on 8th July 2000 for CASE 5, CASE 6, CASE 7, CASE 8 and CASE 9 .

2.2 Sensitivity to air-ice and ice-ocean drag coefficients

Along with *P**, the atmospheric and oceanic drag coefficients have been identified as crucial parameters for sea ice drift. A few sensitivity experiments were performed to obtain the optimal set of the drag coefficients to run the model under more realistic conditions.

We also focused on the regime of the katabatic winds and its impact on sea ice evolution in TNB and on the polynya size. The latter, in fact, is a consequence of the freezing of the water in the bay as a result of a weakening of the katabatic flows or changing in their trajectory (Bromwich and Kurtz, 1984; Priestley, 1914). The duration of the katabatic events have a greater contribution than the intensity and frequency of the katabatic flows in determining the polynya extent (Ciappa et al., 2012; Rusciano et al., 2013). Rusciano et al. (2013) found most frequent katabatic events take place during the winter season and last on average from one to three hours. That means that long time intervals (daily/six hourly) atmospheric input probably misrepresent the real and local atmospheric field in a given temporal period. On the other hand, a single source of AWS data fails to properly reproduce the coastal wind regime resulting from the drainage of the interior katabatic airflows through the different confluence pathways (Petrelli et al., 2008). In view of these considerations, in the next experiments the time resolution was increased so that the model is able to catch any katabatic events. Furthermore a second dataset from AWS Manuela (see section 2.2.1) was taken into account to enlarge the area of influence of the katabatic flows. Unfortunately, no other weather station is available in the southernmost region of the bay and near to the Drygalski Ice Tongue. Also the merging function was modified and the range of influence of the AWS data on the reanalysis data is let to assume an ellipse shape rather than a circumference. This time r is the distance in X and Y from the AWS multiplied by the opposite semi-axis and R is the e-folding length scale specifically given by the product of the semi-axes R1 and R2 of the ellipse with a fixed length. Specifically, in the next runs R1=50 km and R2=20 km for both stations.

Table 6 shows the experiments performed to explore the impact of varying c_{da} and c_{do} parameters, increasing and/or decreasing the one with respect to the other, on sea ice drift. Substantially, an increasing of c_{da} and/or at the same time a decreasing of c_{do} let sea ice to move faster and vice versa.

The first experiment (E_{15}) is the control simulation of one winter month of the year 2005 for which the model has been configured with constant and more commonly used values for the drag coefficients, $c_{da} = 1 \times 10^{-3}$ and $c_{do} = 5 \times 10^{-3}$. In the next experiments the two drag coefficients were let to vary individually or simultaneously with respect to those of the control run. Specifically in the second experiment (E_{35}) c_{da} varies and c_{do} is the same of the control, in the third one (E_{11}) only c_{do} varies while in the fourth (E_{31}) and in the fifth (E_{34}) experiments both two parameters vary together. The sixth experiment ($E_{c_{da}/c_{do}}$), described afterwards, was carried out using non constant values for the drag coefficients. All the experiments are forced with atmospheric forcing from the AWS Manuela at ten minutes resolution combined with hourly data from the AWS Rita. The resulting values are averaged with the six hourly ERA-Interim data so as to adjust the background parameters fields, especially the winds. In addition, the output time of the variables simulated by the model were set equal to 3 hours since, as explained above, this value would appear to be a good compromise to catch katabatic winds.

As the previous sensitivity experiments, a significant dependence of the sea ice simulation on the wind forcing can be inferred from the results of the modelled output fields. The sea ice distribution appears to be very sensitive to the pattern of the wind stress which varies considerably depending on the surface winds. Fig. 6 (top panel) shows the wind velocities and the wind stress for E_{15}, E_{35}, E_{11}, E_{31} and E_{34} experiments. The wind field is the same for all the experiments since they have been forced with the same wind configuration and showing a max values up to 23 m/s and a mean value of 9 m/s. The wind stress which varies depending on the drag parameters, exhibit averages of 0.16, 0.41, 0.13, 0.27 and 0.40 N/m^2 in E_{15}, E_{35}, E_{11}, E_{31}, E_{34}, respectively. The largest values have been found, as expected, in E_{35}, E_{31} and E_{34} with a maximum of 1.48, 1.34 and 1.47 N/m^2 versus much smaller maximum in the CTRL run (E_{15}) and in E_{11} of approximately 0.54 N/m^2.

	Experiment	c_{da}	c_{do}	
1	E_{15} CTRL	1×10^{-3}	5×10^{-3}	-
	E_{35}	3×10^{-3}	5×10^{-3}	
	E_{11}	1×10^{-3}	1×10^{-3}	
	E_{31}	3×10^{-3}	1×10^{-3}	
	E_{34}	3×10^{-3}	4×10^{-3}	
	Ec_{da}/c_{do}	1×10^{-3} $V \leq 10$ m/s 3×10^{-3} $V \geq 20$ m/s	$1.3 \times c_{da}$	
2	Ew_{15}	$= E_{15}$		Wind Enhancement
	Ew_{31}	$= E_{31}$		
	Ew_{34}	$= E_{34}$		
	$Ew_{cda/cdo}$	$= Ec_{da}/c_{do}$		

Table 6: Sensitivity tests with respect to the air-ice and ice-ocean coefficients.

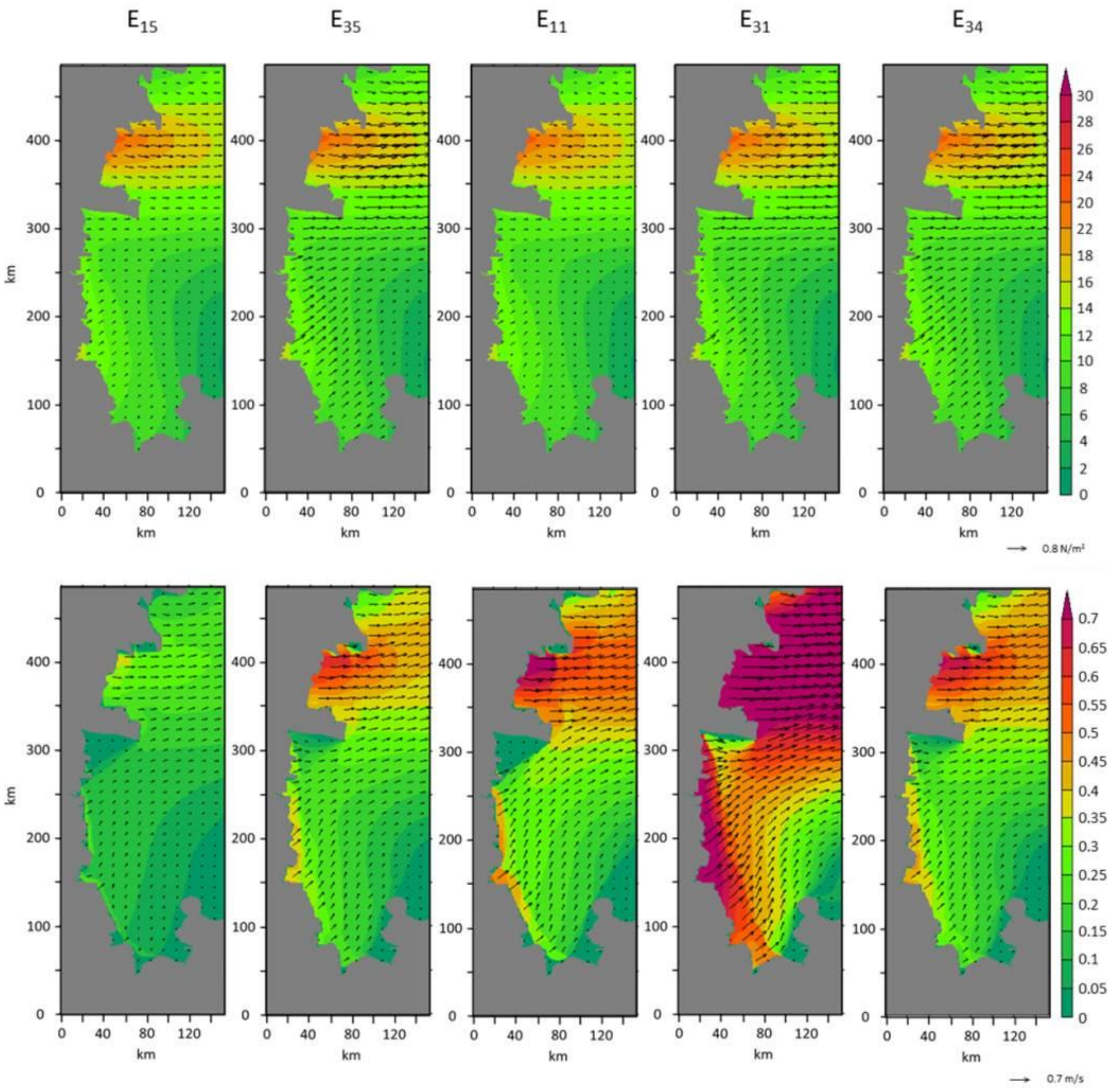

Fig. 6: Wind speed with the superimposed wind stress (on the top) and sea ice drift velocities (on the bottom) on 30[th] July 2005 for E_{15}, E_{35} E_{11} E_{15} E_{31} E_{34} . The scale arrows on the right indicate the length of the wind stress vector and ice velocity vector, respectively 0.8 N/m^2 and 0.7 m/s.

The bigger wind stress in E_{35}, E_{31} and E_{34} leads to maximum ice velocities drift (Fig. 6 bottom) of 0.65, 1.37 and 0.70 m/s respectively; the mean values are 0.23, 0.50 and 0.25 m/s. Maximum and mean values of 0.81 and 0.26 m/s respectively and comparable with those from E_{34} experiment, result from E_{11} where the two coefficients c_{da} and c_{do} differ not much the one from another. Smaller values, as expected, come from E_{15} with a maximum of 0.37 m/s and a mean of 0.12 m/s. Sea ice concentration and thickness maps displayed in Fig. 7 reveals that sea ice distribution, resulting from the modelled wind field and sea ice drift, is well simulated in E_{35}, E_{11} and E_{34} where the gap between c_{da} and c_{do} is small. On the other hand, when c_{do} is much greater than c_{da}, the ice drift becomes unrealistic and too strong also in regions out of the range of the coastal winds or, in the opposite case, really insignificant along shore. These results supports the importance of the c_{da}/c_{do} ratio considered the most basic dynamics parameter determining the mean drift speed (McPhee, 1980; Leppäranta, 1981; Stössel, 1992; Geiger et al., 1998; Harder and Fisher, 1999).

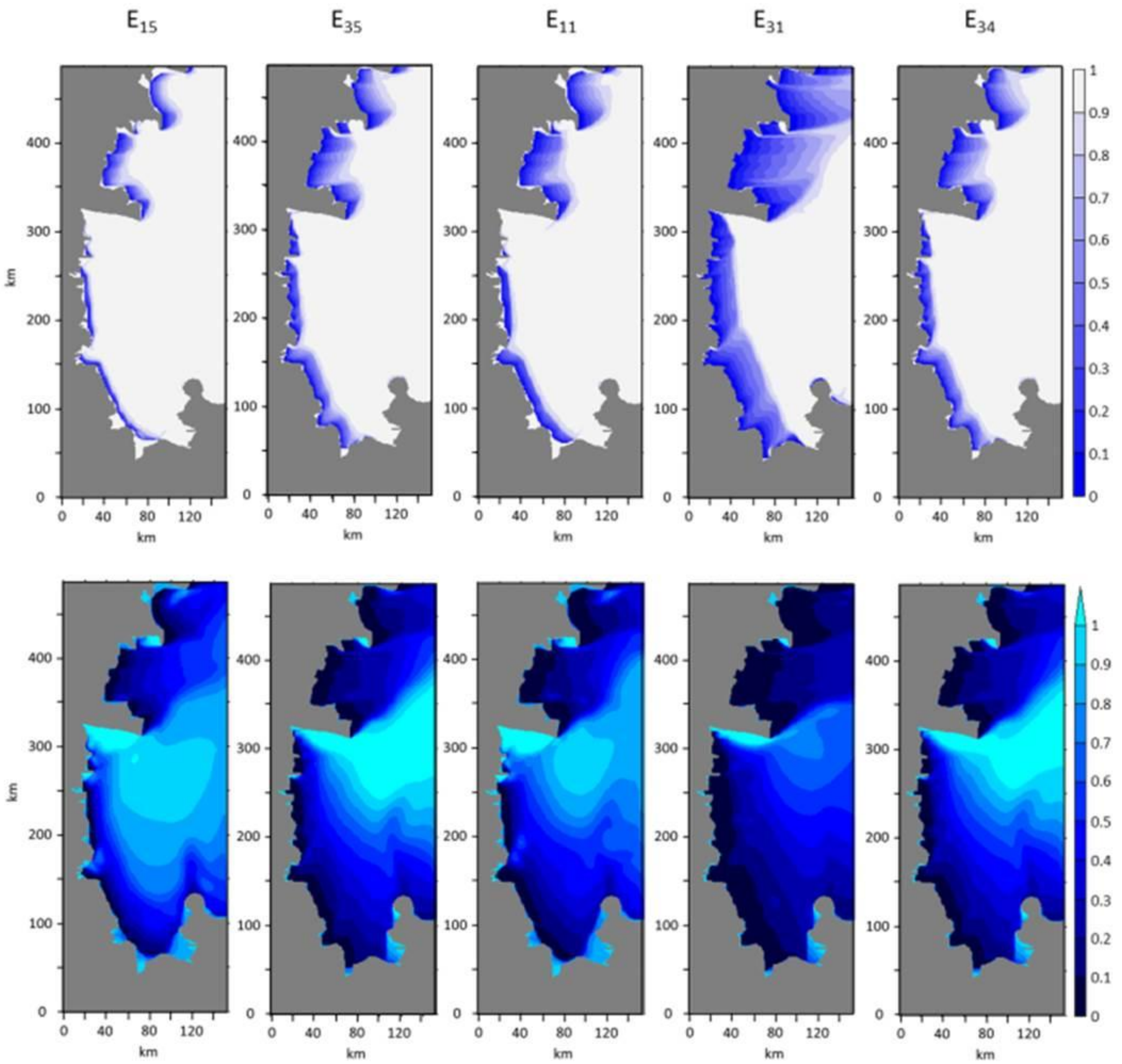

Fig. 7: Sea ice concentration (on the top) and sea ice thickness (on the bottom) on 30th July 2005 for E_{15}, E_{35} E_{11} E_{15} E_{31} E_{34}.

Furthermore, unlike the strength parameter $P*$ which has a strong impact mainly in thick and more compact areas of the pack ice, the c_{da}/c_{do} ratio influences the ice drift in all regions during all season (Kreysher et al., 2000). Therefore, in the last experiment (Ec_{da}/c_{do}), c_{da} was let to vary from 1×10^{-3} for wind speed smaller or equal to 10m/s, and to 3×10^{-3} for wind speed larger or equal to 20 m/s. Then, c_{do} is allowed to depends linearly on the c_{da} through a constant factor of 1.3.

Fig. 8a shows the wind forcing with the superimposed wind stress and the ice velocity (top panel) from the Ec_{da}/c_{do} on the 30th July 2005 at 24.00 and the relative ice concentration and thickness maps (on the bottom). Mean and maximum values of the wind stress are very similar to those resulting from E_{34} showing a maximum of 1.39 N/m^{2}and a mean of 0.30 N/m^2 causing an ice drift with a mean ice velocity of 0.27 m/s with maximum values of 0.71 m/s. A further set of experiments indicated by the number 2 in Table 6 has been performed to deal with the systematic underestimation of the wind speeds especially in coastal areas and near TNB in global reanalysis (Cullather et al., 1997; Fusco et al., 2002; Petrelli et al., 2008). An enhancement function has been designed and applied to improve the prediction of sea ice field. This function represents a correction, varying spatially and differently for both wind components, modifying thus the wind fields in the whole domain. It enhances very strong Era Interim winds, which can be assimilated to katabatic winds allowing very slow ones to be unchanged. Basically the wind vector is multiplied by a function like the following

$$a \cdot \left(1 + \tanh\left(\frac{w - w'}{w''}\right)\right)/2$$

where a is an amplifying factor, tanh is the hyperbolic tangent, w is the x/y wind speed component, while the two parameters w' and w'' (m/s) control for what values of the wind the enhancement occurs and how rapidly the wind enhancement takes place respectively. Suitable values used in the following experiments are a=2, w''=10 while w' has been fixed to 4 and 0 respectively for the eastward and northward component of the wind. However, the wind and ice fields from the Ewc_{da}/c_{do} showed in Fig. 8 b suggest that the wind enhancement function results in unrealistically large wind stress values which go beyond the expected values. In conclusion, the results of Ec_{da}/c_{do} provide the best simulations of the sea ice dynamics of TNB.

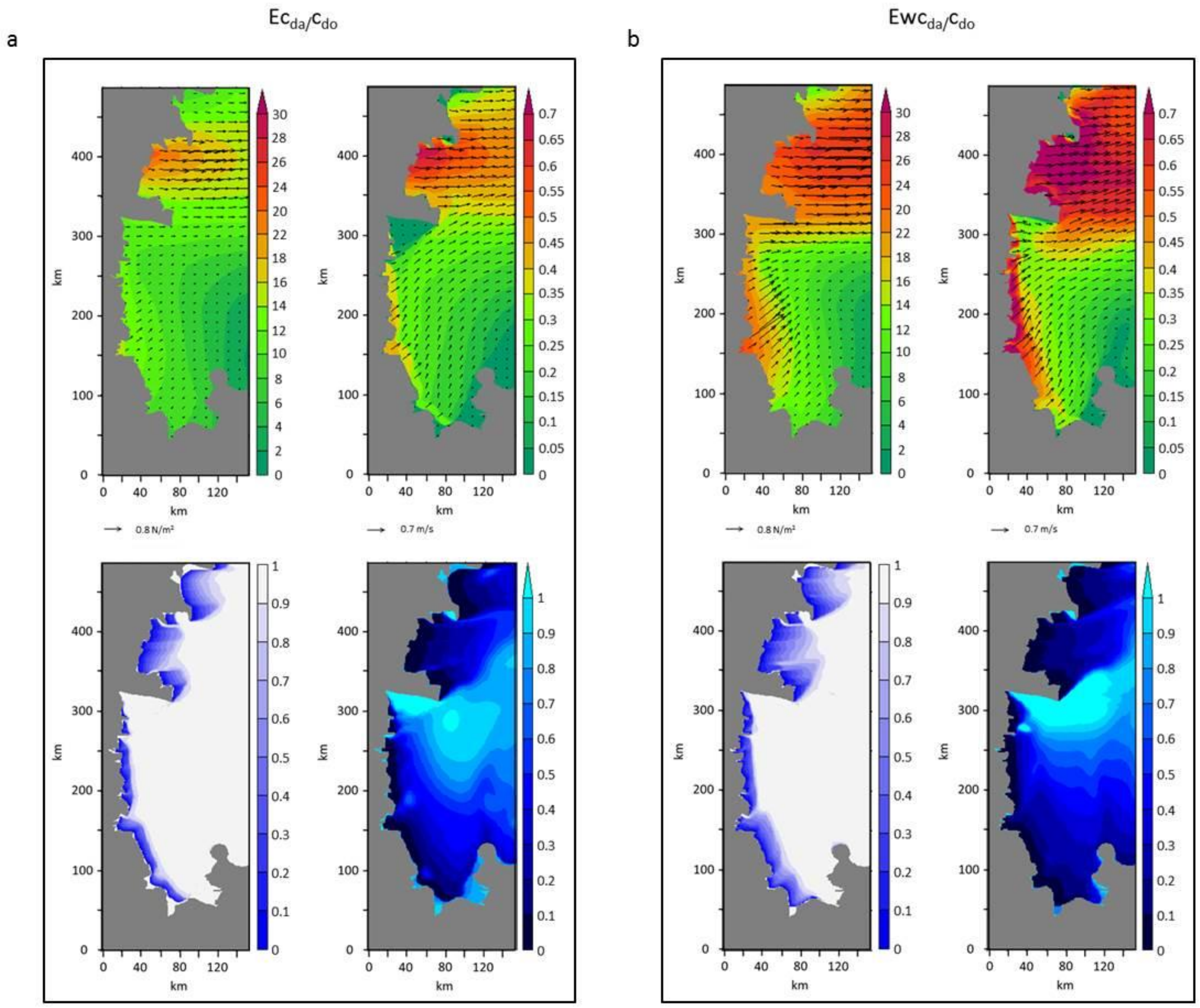

Fig. 8: Wind fields and modelled sea ice drift fields (on the top) and the corresponding sea ice concentration and thickness distribution (on the bottom) on 30th July 2005 for Ec_{da}/c_{do} (a) and Ewc_{da}/c_{do} (b) run without and with the enhancement function respectively.

4 One year numerical simulation and results

One year simulation of TNB sea ice evolution has been carried out to investigate the polynya behaviour in response to the local katabatic flows. The main results of the 2005 simulation are showed.

The modelled polynya behaviour follows the characteristic dynamics of sea ice and ocean circulation in TNB. During the summer season, approximately from November to March, the bay is mostly ice free. It starts to be covered by sea ice in late March, when the low atmospheric and oceanic temperatures let the sea surface freeze. The evolution of the polynya is strongly controlled by the action of katabatic winds which allow TNB to be almost never completely ice covered in winter. Katabatic winds are very intense between April and October (Rusciano et al. 2013), and within this period several cycles of opening/closure of the polynya occurred.

Model-derived polynya extents in TNB area, defined in the section 3.2, have been computed for 2005. The polynya area is usually defined as the sum of the surfaces of open water and thin sea ice and therefore is restricted to the oceanic region within which the ice concentration is smaller than a given threshold (Willmott et al. 2007). This threshold is rather arbitrary varying commonly from 0.5 to 0.7 (Parmiggiani 2006; Kern et al., 2007). An ice concentration threshold of 0.7 has been used here to estimate the TNB polynya extent. A marked dependence of the polynya extent on the wind forcing can be observed (Fig. 9).

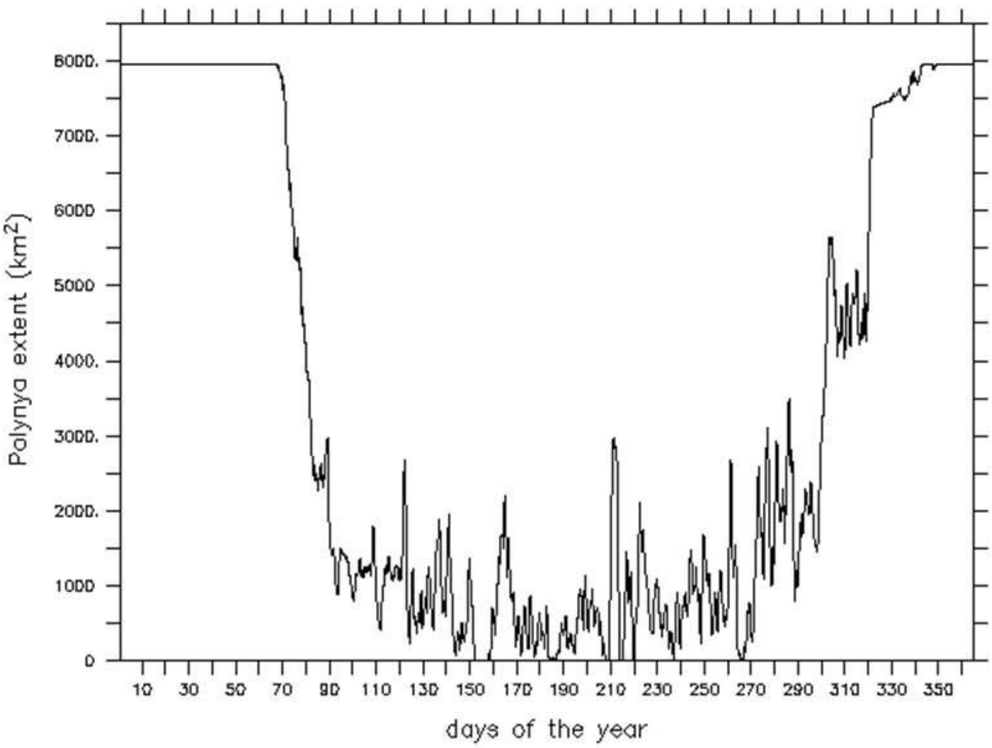

Fig. 9: Model-derived polynya extent in the TNB region in the year 2005.

An increase of the polynya size is associated to the occurrence of katabatic events. The peak extent in midwinter occurred in July with a maximum value of 2962 km^2, followed by other two large extents of the polynya in August and September of 2868 km^2 and 2674 km^2 respectively (Table 7). Polynya mean extents vary approximately from just over 500 km^2 up to almost 900 km^2, except in March/April, when sea ice formation processes start, and in October, which represents the end of the wintertime and the beginning of sea ice melting processes. The computed polynya extents are in good agreement with the wintertime values estimated by Petrelli et al. (2008) and with those recently published by Ciappa et al. (2012) who computed a mean annual open water of around 900 km^2 in the period 2005-2010 and 600 km^2 in 2006 using MODIS thermal infrared data. In any case, the computation of the polynya extent is not trivial since it depends on the accuracy and the limitations of the models and the remote sensing tools, as well as on their capability to resolve in time and in space the processes involved in the polynya variability. In addition, the local coastal winds have a strong but not exclusive impact on the polynya size which is caused by the interaction between katabatic forcing and synoptic weather conditions on longer timescales. The major effect of the katabatic winds on short timescales is the local recirculation of sea ice in TNB and its redistribution within the polynya area (Petrelli et al., 2008). The recirculation forced by these local winds enhances the ice production maintaining high ice production rates in open water and thin ice regions.

Winter months	**Maximum Polynya extent (km^2)**	**Mean Polynya extent (km^2)**
March	7946	5574
April	1806	1174
May	2688	871.2
June	2205	557.2
July	2962	532.5
August	2868	766.9
September	2674	875.6
October	5637	2304

Table 7: Monthly maximum and mean polynya extent of the TNB polynya.

Sea ice production in TNB area (Table 8) has been also computed by model sea ice fields outputs. The ice production rate (Fig. 10), depends primarily on the presence of open water and on the surface wind speeds, therefore following the same trend as the TNB polynya extent. The spatial maximum sea ice production daily rate over TNB area exhibits a maximum of 0.70 km^3/day on 30th July (211th julian day) that is equivalent to 48.08 cm/day. These estimates are comparable to those of Petrelli et al. (2008) who found in high resolution winter experiment an ice production maximum daily rate of 26.4 cm/day. They are quite consistent, even if slightly smaller, with results from Fusco et al. (2002) whose ice production rates for the years 1993 and 1994 show a monthly average of 39 cm/day and a maximum of 72 cm/day in August 1994. Smaller daily rates result in a cumulative ice production value of 39.29 m over the 2005 versus yearly ice production of 81.7 m and 68.8 m for 1993 and 1994 presented in Fusco et al. (2002) and similar values in Kurtz & Bromwich (1985) and Van Woert (1999a, 1999b). These results were obtained using only AWS data, while ice production was already significantly reduced if computed using the ECMWF data. The spatially cumulative daily ice production is also showed in Fig. 11. The highest peaks of ice production occur in May, June and July with the maxima of 0.61, 0.54 and 0.70 km^3 respectively. The cumulative ice production, that is the sea ice volume produced in the whole year 2005, is 57.91 km^3. This value is consistent with the mean value of annual cumulative sea ice production of 59.2$\pm$ 10 km^3 estimated by Tamura et al. (2008) for the TNB polynya. In particular, the ice volume in the months of June and July amounts overall to 16.37 km^3 which is in good agreement with the value of 16.4 km^3 computed by Petrelli et al. (2008) in her winter experiment. The brine rejection (kg/day), associated with the new ice production, and the HSSW production (m^3/day), are also calculated following Markus et al. (1998) and Van Woert (1999a) respectively showed in (Fig. 11).

The salt and HSSW production are larger in wintertime, when the ice production is higher. Their cumulative values in the year 2005 within the TNB polynya are 1.7×10^{12} kg and 0.5×10^{13} m^3 respectively. These values are in good agreement with those of other works even if relative to different years. Fusco et al. (2002), for example, estimated a salt production of about 4.6×10^{12} kg and a HSSW production of 1.5×10^{13} m^3 in the years 1993-94.

Winter months	Maximum daily rates of sea ice production (km^3/day)	Mean daily rates of sea ice production (km^3/day)	Monthly cumulative sea ice (km^3)
March	0.42	0.16	4.99
April	0.40	0.26	7.86
May	0.61	0.30	9.25
June	0.54	0.25	7.52
July	0.70	0.22	6.98
August	0.58	0.30	9.39
September	0.44	0.24	7.34
October	0.39	0.14	4.29

Table 8: Daily sea ice production rates from ice production rates spatially cumulated over TNB polynya area.

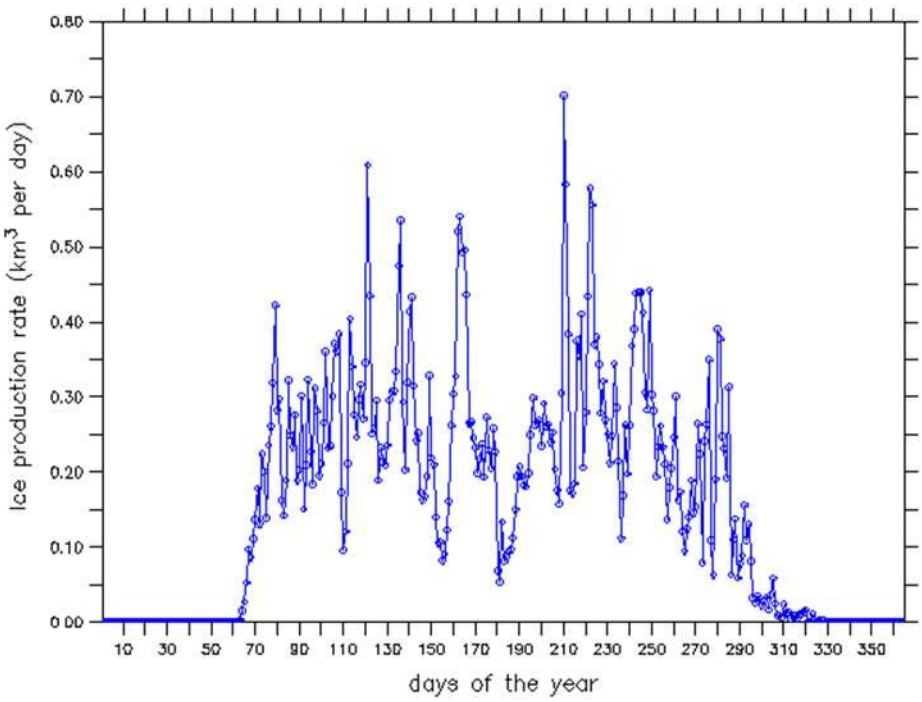

Fig. 10: Spatially cumulated daily rate of sea ice production for the TNB region in the year 2005 .

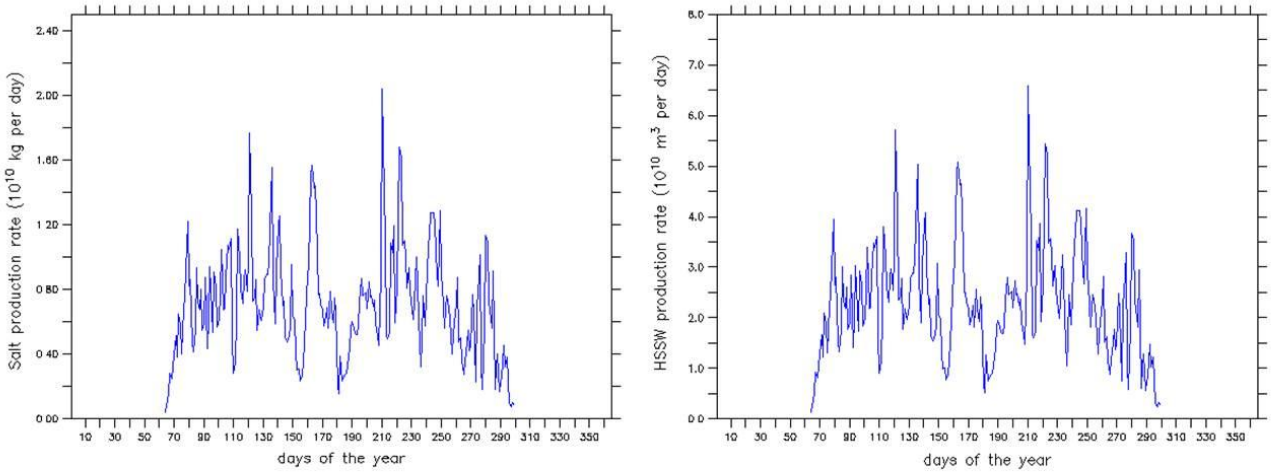

Fig. 11: Salt production rate (on the left) and HWSS production rate (on the right) in the TNB polynya area in the year 2005.

5 Model comparison with MODIS data

In situ measurements are particularly poor in remote or hardly accessible areas during the Antarctic winter, therefore satellite observations represent a useful tool in tuning numerical simulations of the coupled models (Linch et al., 1997). Satellite images in combination with numerical weather prediction model data and in situ data from Automatic Weather stations provide a good database to study polynya-atmosphere interactions in TNB area (Gallée, 1997; Ciappa et al., 2012).

Whereas true measurements of ice thickness and then total ice volume in Terra Nova Bay are not available, the model-derived polynya extent was compared to satellite images. Particularly, the NASA's MODIS (Moderate Resolution Imaging Spectroradiometer) sensor provides high temporal and spatial resolution measurements of Earth's land, ocean and atmospheric processes in several spectral bands and swath. The MODIS/Aqua Level 1B 1km Calibrated Radiances at 1 km resolution have been used to retrieve the ice surface temperature (IST) in the TNB region and subsequently to derive the polynya extent. Radiance data from MODIS channels 31 and 32 are converted to brightness temperatures (Kelvins) through the inversion of the Planck's law equation

(Key et al., 1994). For ice/snow surface temperature (IST) computation the equation based on the technique of Key et al. (1997), originally developed for the Advanced Very High Resolution Radiometer (AVHRR), is used.

In order to support the dependence of the opening/closing cycles of the polynya on the wind forcing, a few significant periods in the wintertime of 2005 characterized by stronger katabatic events have been identified. For each period sea ice concentration maps from ice fields model outputs have been produced. The polynya edge is identified by the first contour line characterized by an ice concentration threshold of 0.7. These maps have been compared with MODIS IST images obtained following the aforementioned procedure for the same period.

Fig. 12 and Fig. 14 show the wind speed from both Rita and Manuela AWSs during two katabatic events observed in May and July (1-5 May and 28-31 July respectively). The evolution of the polynya extent detected by MODIS can be observed in Fig. 13 and Fig. 15 where the modelled sea ice concentration for the same days is also showed. Sea ice concentration maps at the temporal steps closer to those of satellite scenes have been chosen to match at the best model and MODIS products.

The model seems to reproduce reasonably sea ice dynamics as shown by the similar polynya behaviour in both sea ice concentration and IST maps. The drift of sea ice responds to wind forcing which shows a predominant West-West Nord West direction. Stronger winds are responsible for sea ice advection offshore, opening the polynya, and contributing to increase its extent, while weaker winds just hamper the closure keeping the polynya opened. According to Pease (1987), a seaward wind component exceeding 10m/s is sufficient to maintain a polynya in coastal zones. Our results are in agreement with the suggested threshold.

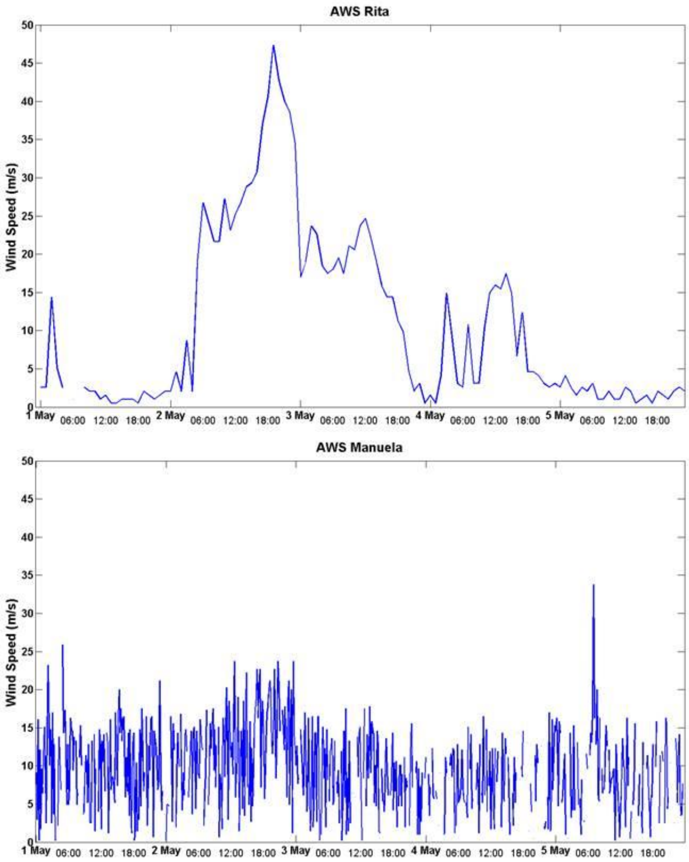

Fig. 12: Wind speed from Rita (on the top) and Manuela (on the bottom) AWSs on 1-5th May 2005.

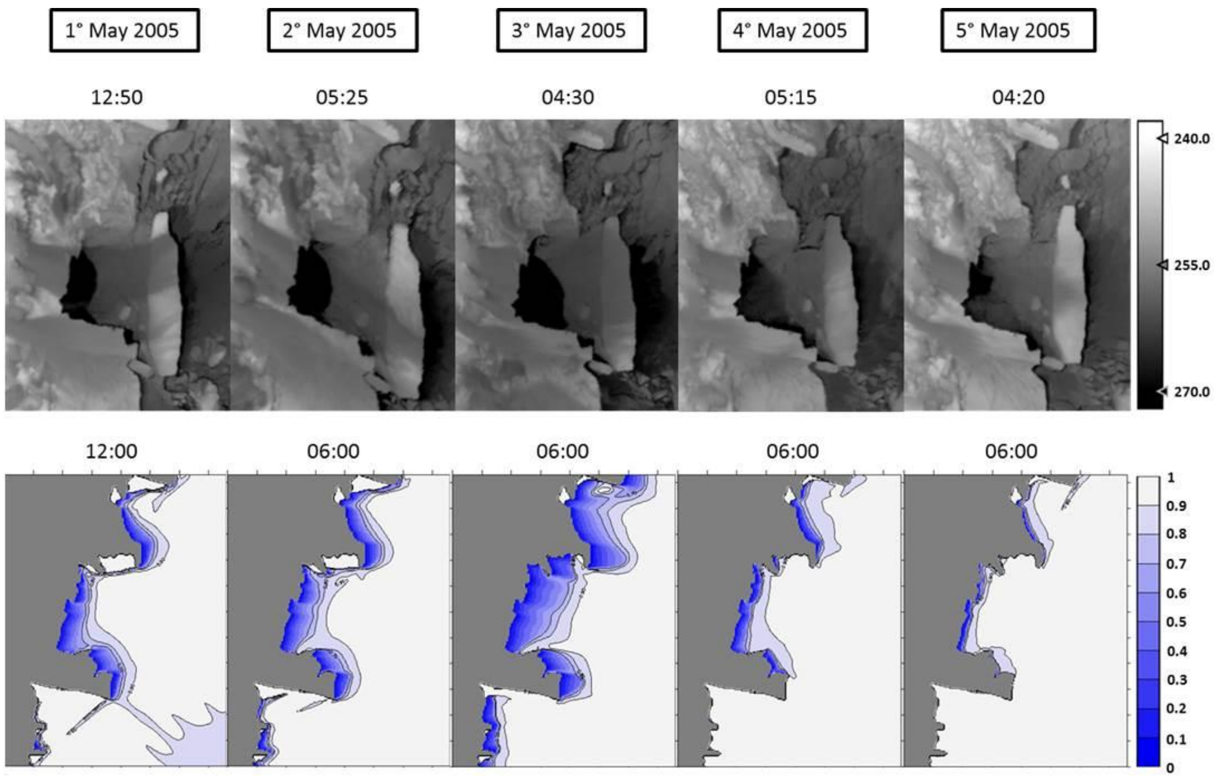

Fig. 13: IST MODIS scenes (on the top) and the modelled sea ice concentration maps (on the bottom) displaying the polynya evolution on 1-5th May 2005.

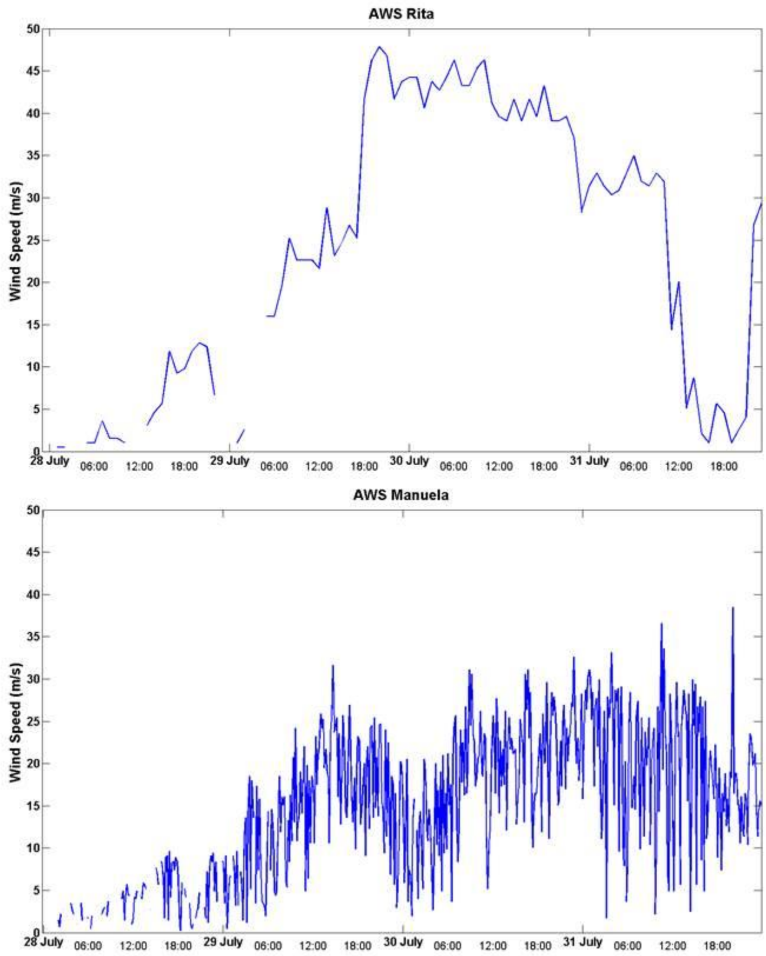

Fig. 14: Wind speed from Rita (on the top) and Manuela (on the bottom) AWSs on 23-31[th] July 2005.

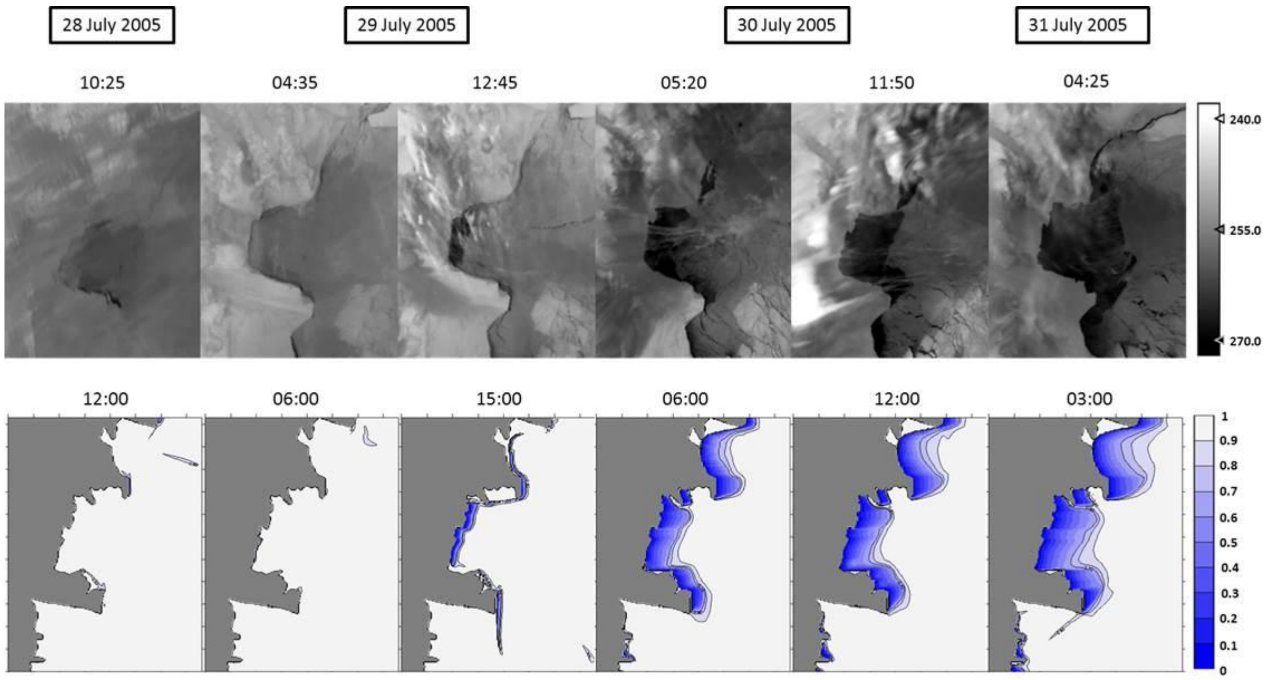

Fig. 15: IST MODIS scenes (on the top) and the modelled sea ice concentration maps (on the bottom) displaying the polynya evolution on 23-27[th] July 2005.

The small polynya observed at the beginning of the 1st of May (Fig. 13) increases its extent on 2nd day of the month upon an increase of the wind speed measured by the AWS Rita, exhibiting a value well over 20 m/s reaching a peak of almost 50 m/s. Wind speed from the AWS Manuela with an average value of 20 m/s contribute to enlarge the polynya eastward. The polynya size keeps on increasing at the beginning of 3rd of May until the wind speed drops sharply, below 10 m/s for AWS Rita, and the polynya starts closing on 4th and 5th of May. The small discrepancies between the spatial distribution of sea ice in model simulations and IST MODIS scenes are thought to be due to the iceberg B-15A drifting in front of the TNB approximately in April-May 2005. The presence of this iceberg blocks the drift of sea ice offshore leading the ice to accumulate in its proximity. In fact, in IST MODIS scenes the edge of the polynya is located more toward the coast and southward reducing thus the northern portion of the whole polynya extent. The simulation of sea ice distribution in July 2005 (Fig. 15) shows a higher degree of similarity with that observed in satellite images probably since the advection of sea ice is less affected by the iceberg moving out of the bay. On 28th July the polynya is almost totally closed because of the wind speeds are near to zero. After an enhancement of the wind forcing the polynya starts opening at the beginning of the 29th of July and expands rapidly seaward. The largest opening of the polynya occurs on 31 July 2005 in response to the stronger wind speeds values recorded previously by AWS stations, near to 50 m/s for Rita and 40 m/s for Manuela. Some discrepancies between the simulated polynya and that observed in MODIS scenes may probably due to the gaps (missing data) in the AWSs wind datasets.

The modelled polynya extents have been also computed for both MODIS IST scenes and sea ice concentration maps on 28-31 July. The aforementioned sea ice concentration threshold of 0.7 has been used for the modelled ice. A varying threshold for IST proposed by Ishikawa et al. (1996) and Zwally et al. (1983) that discriminates open water and thin ice from thick ice or land fast ice has been employed for satellite maps. Setting sea ice concentration to 0.7, our IST threshold is given by $T_{th} = 0.3T_f + 0.7T_{ice}$ where T_f is the temperature of the open water at the freezing point and T_{ice} is the temperature of sea ice around the polynya. Both the temperature values are extracted from the IST scenes after they have been visually inspected one by one. In particular, T_f is given by the warmest IST found within the polynya and T_{ice} is estimated as the average of the IST values found around the open water.

Polynya extents from the 28th July to the 31th July, present the largest opening of the whole of 2005, as also found in Ciappa et al. (2012), and are showed in Table 9. The model-derived polynya extents mostly agree with those computed from MODIS IST images revealing the same temporal trend in polynya increasing during the observed katabatic event. The polynya extent values are less comparable to the MODIS based extents retrieved by Ciappa et al. (2012) showing a polynya extent of approximately 7615 km^2 on 31 July at 4:25 versus the corresponding MODIS-derived and model-derived polynya extents of 3393 km^2 and 2831 km^2 respectively. That is due to the wider domain considered in his estimates, including all the open water fraction occurred north of TNB (Wood Bay) and south of the Drygalski Ice Tongue.

TNB polynya event in July 2005	Model-derived polynya extent (km^2)	MODIS-derived polynya extent (km^2)
28th 12:00	12	40
29th 06:00	0	25
29th 15:00	389	391
30th 06:00	1858	1936
30th 12:00	2148	2385
31th 03:00	2831	3393

Table 9: TNB polynya extents from model sea ice concentration outputs and from MODIS IST from 28th to 31th July 2005.

6 Discussion and concluding remarks

This work focuses on the investigation of sea ice formation in the TNB polynya in response to wind forcing. Because of the lack of direct observations related to sea ice fields, models provide valuable insight into the mean state of the ice cover (Flato, 2003) together with satellite observations which indeed fail often in availability and spatial resolution. A coupled sea ice-ocean model that simulates the seasonal cycle of sea ice formation in, and export off, the polynya is presented. The model consists in a one-and-a-half layer reduced gravity ocean in which the oceanic dynamics satisfy the hydrostatic equilibrium and the Boussinesq approximation. Vertical mixing in the ocean is prescribed according to the parameterization of Pacanowski and Philander (1981). The model allows for the presence of a sea ice cover which behaves as a zero layer system without thermal inertia, as proposed by Semtner (1976), interacting dynamically and thermodynamically with the atmosphere and the ocean. The model also allows for internal ice forces resolved by the elastic-viscous-plastic ice rheology developed by Hunke and Dukowicz (1997). Vertical and lateral growth/decay rates of sea ice are obtained from energy budgets at both the bottom and surface boundaries of the ice cover and in leads opening within the ice cover. Also, snow-ice formation is prescribed when the load of snow is large enough to depress the snow–ice interface under the water level. The model is applied to TNB area, including also the nearby regions north and south of the bay in order to characterize at the best seasonal sea ice variability and polynya behaviour. The horizontal resolution is of 1 km, which is sufficient to represent the salient features of the coastline geometry, notably the Drygalski Ice Tongue. The model has been forced by a combination of Era Interim reanalysis by ECMWF and in-situ data from Rita and Manuela AWS, and also by in situ oceanic data.

The modelled sea ice fields have proved to be very sensitive to the atmospheric forcing. Sea ice evolution has been found to be shaped by different parameters involved in the dynamics of sea ice which in turn affects the thermal processes that occur in the ice cover. Several sensitivity experiments have been performed in order to optimize and set up a few main parameterizations and coefficients, thus improving the model outputs. The choice of an ice thickness collection depth (H) varying with the wind speed used by Winsor & Björk (2000) has revealed the best compromise in simulating sea ice fields and thermodynamic heat losses through thin ice inside the polynya. In contrast, the rheology parameter P^* has not been found to affect significantly the drift of sea ice resulting in almost unchanged outputs of sea ice concentration and thickness distribution. The importance of the air drag coefficient, one of the most important factors in modelling ice motion, has been also stressed. First the response of the model to constant values of the air-ice (c_{da}) and ice-ocean (c_{do}) drag coefficients and after to the c_{da}/c_{do} ratio have been observed, the latter being the most basic parameter of sea ice dynamics determining the mean sea ice drift speed (Geiger et al., 1998; Harder and Fisher, 1999). For this reason a c_{da} varying with wind speed has been defined, while c_{do} is allowed to depend linearly on the c_{da} through a constant factor. Also a wind enhancement function has been developed in order to try to improve the prediction of sea ice fields. However, its application has revealed no progress in model forcing causing too much high values of the wind stress.

A simulation of sea ice formation in TNB has been performed for the whole of 2005 to observe the response of the polynya dynamics to the wind forcing. Unsurprisingly, the largest openings of the polynya match the stronger katabatic winds which have been found in wintertime, mainly from April to October. The largest opening of polynya occurs in July with an extent of 2962 km^2, while mean polynya extent over the wintertime 2005 ranges between approximately 500 km^2 and 900 km^2. Sea ice production and the associated brine and HSSW productions have also been computed exhibiting values cumulated over the whole year 2005 of 57.91 km^3, 1.7×10^{12} kg and 0.5×10^{13} m^3 respectively. These results are in good agreement with those by Fusco et al. (2002, 2009) who estimated, even if related to different period (1993-94), a salt production of about 4.6×10^{12} kg and a HSSW production of 1.5×10^{13} m^3. In order to support and validate the model outputs, a comparison with sea ice conditions detected by satellite images has been thought essential. Satellite images detected from MODIS sensor have been chosen for this purpose since they reach a high spatial resolution of 1 km, the same as that of the model. In order to observe the strong relationship between the wind field and the TNB polynya extent, some wintertime periods including significant katabatic events have been selected. For these periods the MODIS IST scenes have been compared with the modelled sea ice concentration maps. The TNB polynya area seems to be reproduced reasonably well by the model in terms of both shape and distribution of sea ice. However, small differences in sea ice distribution respect to that observed in the MODIS IST scenes are visually detectable in some regions. These differences involve especially the areas located along the coast characterized by the variable shelf-ice borders and the presence of land fast ice. In particular, two given areas, the region south of Drygalski Ice Tongue and the one north of TNB (Wood Bay) appear almost recurrently ice free in the modelled sea ice maps.

The modelled polynya extents in MODIS IST scenes and the corresponding model sea ice maps have been also computed from 28th to 31th July 2005. The application of an ice state dependent threshold for IST in MODIS images let us to validate the polynya extent with a higher reliability. The model-derived polynya extents are very similar to those computed from MODIS IST images. The extent value of 2831 km^2 computed from the modelled ice concentration for the 31th July at 3:00 is quite consistent with that obtained from the MODIS scenes of 3393 km^2 for the same day at 4:25. On the other hand, both extents are much smaller and, hence, less comparable to MODIS based estimation of 7615 km^2 retrieved by Ciappa et al. (2012) on the same day because of the wider area considered in his work including the open water fraction also north of TNB (Wood Bay) and south of the Drygalski Ice Tongue.

Finally, despite the small discrepancies in sea ice distribution in some given regions and polynya extents, the model works quite well reproducing reasonably sea ice evolution. The divergences may be investigated more extensively in the future through an improvement of the model in capturing fast ice or the use of a more accurate land mask including the fast ice. The detection of the polynya area and its extent is obviously affected by fog, clouds or other atmospheric disturbance that often compromise the quality of the used satellite images. At any rate, modelling the opening and closing polynya events is a difficult task especially if the size of polynya is relatively small, like in Terra Nova Bay (Pease, 1987; Lynch et al., 1997; Petrelli et al, 2008). The results have further highlighted the sensitivity of sea ice simulations to wind forcing which is the major aspect stressed in numerous modelling works on Southern Ocean. Accurate sea ice simulations in terms of sea ice distribution and thickness can be achieved, provided that the model is forced with realistic winds and lower boundary conditions, in particular ocean temperatures as found by Stössel et al. (2011). High resolution wind forcing is necessary to capture in more detail coastal sea ice processes, such as coastal polynyas, ice drift and ice compression against some particular coastline features.

Acknowledgments

The authors are thankful to the Meteo-Climatological Observatory of the Italian National Program for Research in Antarctica and the Antarctic Meteorological Research Center of the University of Wisconsin-Madison for the Automatic Weather Stations data sets. They are also grateful to the European Centre for Medium-range Weather Forecast for the interim reanalysis and to the MODIS Atmosphere and Archive and Distribution System Nasa Website for free access to MODIS radiance products. This work was performed in the framework of CEFA (PNRA) project.

References

Bromwich D. H. 1989: An extraordinary katabatic wind regime at Terra Nova Bay, Antarctica, Mon Weather Rev., 117 (3), 688-695.

Budillon, G., Fusco, G., & Spezie, G., 2000: A study of surface heat fluxes in the Ross Sea (Antarctica). Antarctic Science, 12(2), 243–254.

Ciappa A., Pietranera L., and Budillon G., 2012: Observations of the Terra Nova Bay (Antarctica) polynya by MODIS ice surface temperature imagery from 2005 to 2010, Remote Sens. Environ., 119, 158–172.

Connolley W. M., Gregory J. M., Hunke E. C. and McLaren A. J., 2004: On the consistent scaling of terms in the sea ice dynamics equation. J. Phys. Oceanogr., 1776–1780.

Cullather R. I., Bromwich D. H. and Grumbine R.W., 1997: Validation of operational numerical analyses in Antarctic latitudes. J. Geophys. Res., 102, 13761-13784.

Darby M. S., Willmott A. J. and Mysak L. A., 1994: A nonlinear steady-state model of the North Water Polynya, Baffin Bay. Journal of Physical Oceanography, 24,1011-1020.

Darby M. S., Willmott A. J. and Somerville T. A., 1995: On the influence of coastline orientation on the steady state width of a latent heat polynya. J. Geophys. Res., 100, 13,625-13,633.

Gallée H., 1997: Air-sea interactions over Terra Nova Bay during winter simulation with a coupled atmosphere-polynya model, J. Geophys. Res., 102(D12), 13,835-13,849.

Geiger C. A., Hibler W. D. and Ackley S. F., 1998: Large-scale sea ice drift and deformation: Comparison between models and observations in the western Weddell Sea during 1992, J. Geophys. Res., 103(C10), 21,893-21,913.

Fichefet T. and Morales Maqueda M.A., 1999: Modelling the influence of snow accumulation and snow-ice formation on the seasonal cycle of the Antarctic sea-ice cover. Clim. Dyn., 15, 251–268.

Flato G. M., 2003: Sea Ice Modelling. Chapter 9 in Mass Balance of the Cryosphere: Observations and Modelling of Contemporary and Future Changes, eds. J. Bamber and A. Payne, Cambridge University Press, pg. 367-389.

Frezzotti, M., and M. C. G. Mabin, 1994: Twentieth century behavior of Drygalski Ice Tongue, Ross Sea, Antarctica, Ann. Glaciol., 20, 397–400.

Feltham, D.L. 2008. Sea ice rheology. Annu. Rev. Fluid Mech., 40, 91–112.

Fusco G., Flocco D., Budillon G., Spezie G., Zambianchi E., 2002: Dynamics and Variability of Terra Nova Bay Polynya, Marine Ecology, 23, 201-209.

Fusco G., Budillon G., Spezie G., 2009: Surface heat fluxes and thermohaline variability in the Ross Sea and in Terra Nova Bay polynya, Cont. Shelf Res. 29, 1887-1895.

Harder, M. and Fischer H., 1999: Sea ice dynamics in the Weddell Sea simulated with an optimized model, J. Geophys. Res., 104, 11,151-11,162.

Hibler W. D. III, 1979: A dynamic thermodynamic sea ice model, J. Phys. Oceanog., 9, 815–846.

Hibler, W. D., III and Walsh J. E., 1982: On modeling the seasonal and interannual fluctuations of Arctic sea ice, J. Phys. Oceanogr., 12, 1514 – 1523.

Holland Paul R., Kwok R., 2012: Wind-driven trends in Antarctic sea-ice drift, Nature Geoscience 5, 872-875.

Hunke E. C. and J. K. Dukowicz 1997: An elastic-viscous-plastic model for sea ice dynamics, J. Phys. Oceanogr., 27, 1849-1868.

Ishikawa, T., Ukita, J., Ohshima, K. I., Wakatsuchi, M., Yamanouchi, T., & Ono, N., 1996: Coastal polynyas off East Queen Maud Land observed from NOAA AVHRR data, Journal of Oceanography, 52, 389–398.

Jacobs S. S. and Comiso J. C., 1997: Climate variability in the Amundsen and Bellingshausen Seas. J. Clim. 10, 697–709.

Jacobs S.S., Fairbanks R.G. and Horibe Y., 1985: Origin and evolution of water masses near the Antarctic continental margins: evidence from H2 18O/ H2 16O ratios in seawater, Antarct. Res. Ser., 43, 59-85.

Jacobs S. S. and Comiso J. C., 1989: Sea ice and oceanic processes on the Ross Sea continental shelf. J. Geophys. Res., 94, 18195-18211.

Jacobs S. S. and Comiso J. C., 1997: Climate variability in the Amundsen and Bellingshausen Seas. J. Clim. 10, 697–709.

Jacobs S.S., 2004: Bottom water production and its links with the thermohaline circulation, Antarct. Sci. 16 (4), 427–437.

Key J. R., Maslanik J. A., Papakyriakou T., Serreze M. C. and Schweiger A. J., 1994: On the Validation of Satellite-Derived Sea Ice Surface Temperature, Arctic, 47, 3, 280-287.

Key J. R., Collins J. B., Fowler C. and Stone R. S., 1997: High Latitude Surface Temperature Estimates From Thermal Satellite Data, Remote Sens. Environ., 61, 302-309.

Kern S., Spreen G., Kaleschke L., DE LA Rosa S., and Heygster G., 2007: Polynya Signature Simulation Method polynya area in comparison to AMSR-E 89 GHz sea-ice concentrations in the Ross Sea and off the Adélie Coast, Antarctica, for 2002–05: First results, Ann. Glaciol., 46, 409–418.

Kreysher M., Harder M., Lemke P. and Flato G. M., 2000: Results of the Sea-Ice Model Intercomparison Project: Evaluation of sea ice rheology schemes for use in climate simulations. J. Geophys. Res., 105(C5), 11,299–11,320.

Kurtz D. D. and Bromwich D. H., 1983: Satellite observed behavior of the Terra Nova Bay polynya. J. Geophys. Res., 88, 9717-9722.

Kurtz D. D. and Bromwich D. H., 1985: A recurring, atmospherically forced polynya in Terra Nova Bay. In Oceanology of the Antarctic Continental Shelf, Antarct. Res. Ser., 43, edited by S. S. Jacobs, 177-201, AGU, Washington, D.C.

Lefebvre W. and Goosse, H., 2005: Influence of the Southern Annular Mode on the sea ice-ocean system: The role of the thermal and mechanical forcing. Ocean Sci. 1, 145–157.

Lemke P., 1987: A Coupled One-Dimensional Sea Ice-Ocean Model, J. Geophys. Res., 92(C12), 13,164–13,172.

Leppäranta, M., 1981: On the structure and mechanics of pack ice in the Bothnian Bay, Finnish Mar. Res., 248, 3–86.

Liu J. P., Curry J. A. and Martinson D. G., 2004: Interpretation of recent Antarctic sea ice variability, Geophys. Res. Lett. 31, L02205.

Liu J. P. & Curry J. A., 2010: Accelerated warming of the Southern Ocean and its impacts on the hydrological cycle and sea ice, Proc. Natl Acad. Sci. USA 107, 14987–14992.

Lynch A. H., Glueck M. F., Chapman W. L., Baily D. A. and J. E. Walsh, 1997: Satellite observation and climate system model simulation of the St. Lawrence Island Polynya, Tellus, 2, 277-297.

Maksym, T., S.E. Stammerjohn, S. Ackley, and R. Massom. 2012. Antarctic sea ice—A polar opposite? Oceanography 25(3):140–151,

Markus, T., Kottmeier C. and Fahrbach E., 1998: Ice formation in coastal polynyas in the Weddell Sea and their impact on oceanic salinity, in Antarctic Sea Ice: Physical processes, interaction, and variability, Antarct. Res. Ser., vol. 74, edited by M. O. Jeffries, pp. 273 – 292, AGU, Washington, D. C..

Maykut, G.A. 1978. Energy exchange over young sea ice in the central Arctic. J. Geophys. Res., 83(C7), 3646-3658.

Martinsen E. A. and Engedahl H., 1987. Implementation and testing of a lateral boundary scheme as an open-boundary condition in a barotropic ocean model. Coastal Eng. 11, 603–627.

McPhee, M. G., 1980: An analysis of pack ice drift in summer, in Sea Ice Processes and Models, edited by R. S. Pritchard, Univ. of Wash. Press, Seattle, 62-75.

Mellor G. L. and Kantha L., 1989: An ice-ocean coupled model, J. Geophys. Res., 94, 10,937-10,954.

Morales Maqueda M. Á., Wilmott A. J. and Darby M. S., 1999: A numerical model for intercadal variability of sea ice cover in the Greenland-Iceland-Norwegian Sea, Clymate Dynamics, 15: 89-113.

Morales Maqueda M. Á., Willmott A. J., Biggs N. R. T., 2004: Polynya Dynamics: A review of observations and modelling, Reviews of Geophysics, 42, RG1004.

Mellor G. L. and Kantha L., 1989: An ice-ocean coupled model, J. Geophys. Res., 94, 10,937-10,954.

Olason E. O., and Harms I., 2010: Polynyas in a dynamic-thermodynamic sea-ice model, The Cryophere, 4, 147-160.

Orsi A. H., Johnson G. C. and Bullister J. L., 1999: Circulation, mixing and production of Antarctic bottom water, Progress in Oceanography, 43, Pergamon, 55–109.

Ou H. W., 1988: A time-dependent model of a coastal polynya, J. Phys. Oceanogr., 18, 584–590.

Owens W. B., Lemke P., 1990: Sensitivity studies with a sea ice-mixed layer-pycnocline model in the Weddell Sea. J. Geophys. Res., 95, C6, 9527-9538.

Pacanowski R. and Philander S.G.H., 1981: Parameterization of vertical mixing in numerical models of tropical oceans, J. Geophys. Res. 11, 1443–1451.

Parkinson C. L. and Cavalieri D. J., 2012: Antarctic sea ice variability and trends, 1979-2010, The Cryosphere, 6, 871–880.

Parmiggiani, F. 2006: Fluctuations of Terra Nova Bay polynya as observed by active (ASAR) and passive (AMSR-E) microwave radiometers, Int. J. Remote Sensing, 27(12), 2459–2467.

Pease C. H., 1987: The size of wind-driven coastal polynyas, J. Geophys. Res., 92, 7049–7059.

Petrelli P., Bindoff N. L. and Bergamasco A., 2008: The sea ice dynamics of Terra Nova Bay and Ross Ice Shelf Polynyas during a spring and winter simulation, J. Geophys. Res., 113.

Rothrock D. A., 1979: Modeling sea-ice features and processes, Journal of Glaciology, 24, 90.

Rusciano E., Budillon G., Fusco G., and Spezie G., 2013: Evidence of atmosphere-sea ice-ocean coupling in the Terra Nova Bay polynya (Ross Sea-Antarctica), Continental Shelf Research 61-62, 112-124.

Russell J.L., Stouffer R.J., and Dixon K.W., 2006: Intercomparison of the Southern Ocean circulations in IPCC coupled model control simulations, J. Clim. 19:4,560–4,575.

Semtner A. J., 1976: A model for the thermodynamic growth of sea ice in numerical investigations of climate, J. Phys. Oceanogr., 6, 27–37.

Steele, M., J. Zhang, D. Rothrock and H. Stern. 1997. The force balance of sea ice in a numerical model of the Arctic Ocean. J. Geophys. Res., 102(C9), 21,061–21,079.

Stössel A., Lemke P. and Owens W.B., 1990: Coupled sea ice-mixed layer simulations for the Southern Ocean, J. Geophys. Res., 95, 9539-9555.

Stössel A., 1992: Sensitivity of the Southern Ocean sea-ice simulations to different atmospheric forcing algorithms, Tellus A, 395-413.

Stössel A., Zhang Z., and Vihma T., 2011: The effect of alternative real-time wind forcing on Southern Ocean sea-ice simulations, J. Geophys. Res., 116, C11021.

Tamura T., Ohshima Kay I. and Nihashi S., 2008: Mapping of sea ice production for Antarctic coastal polynyas, J. Geophys. Lett., 35.

Trumbore S.E., Jacobs S. S. and Smethie JR W. M., 1991: Chlorofuorocarbon evidence for rapid ventilation of the Ross Sea. Deep-Sea Research, 38, 845-870.

Turner J., Comiso J. C., Marshall G. J., Lachlan-Cope T. A., Bracegirdle T., Maksym T., Meredith M. P., Wang Z., and Orr A., 2009: Non-annular atmospheric circulation change induced by stratospheric ozone depletion and its role in the recent increase of Antarctic sea ice extent, Geophys. Res. Lett., 36, L08502.

Van Woert M. L., 1999a: The wintertime expansion and contraction of the Terra Nova Bay polynya. In Oceanography of the Ross Sea: Antarctica, edited by G. Spezie and G. M. R. Manzella, pp. 145-164, Springer-Verlag, New York.

Van Woert M. L., 1999b: Wintertime dynamics of the Terra Nova Bay polynya. J. Geophys. Res., 104, 7753-7769.

Willmott A. J., Holland D. M. and Morales Maqueda, M. A., 2007: Polynya modelling. In: Smith, Walker, O.; Barber, David, G., (eds.) Polynyas: windows to the world. Amsterdam, Elsevier, 87-125. (Elsevier Oceanography Series, 74).

Winsor P. and Björk G., 2000: Polynya activity in the Arctic Ocean from 1958 to 1997, J. Geophys. Res., Oceans 105, 8789-8803.

Winsor P. and Björk G., 2000: Polynya activity in the Arctic Ocean from 1958 to 1997, J. Geophys. Res., Oceans 105, 8789-8803.

Zhang J, 2007: Increasing Antarctic Sea Ice under Warming Atmospheric and Oceanic Conditions, *J. Climate*, 20, 2515–2529.

Zwally H. J., Comiso J. C., Parkinson C. L., Campbell W. J., Carsey F. D., and Gloersen P., 1983: Antarctic Sea Ice, 1973–1976: Satellite Passive-Microwave Observations,Washington, DC, National Aeronautics and Space Administration, 206 pp.

Parameter	Symbol	Value
X domain	X	154000 m
Y domain	Y	488000 m
T domain	T	x^* days
Time step for momentum	Δt	600 s
Time step for advection	Δta	1.2 s
Elastic timescale	Δte	180 s
Air drag coefficient	C_{da}	x^*
Ocean drag coefficient	C_{do}	x^*
Ice strength parameter	P^*	x^* N/m^2
Ice concentration parameter	C	20
Creep limit	c	5×10^{-11} 1/s
Eccentricity of the elliptical yield curve	e	2
Demarcation ice thickness	h_{pu}	x^* m

Table 1: Input parameters for the model user

Parameter	Symbol	Value
Thermal conductivity of sea ice	κi	2.2 W/m/K
Thermal conductivity of snow	κ_s	0.3 W/m/K
Emissivity of atmosphere	ε_a	0.95
Emissivity of ocean	ε_o	0.985
Albedo of ocean	α_o	0.07
Albedo of ice	α_i	0.07-0.7
Albedo of snow	α_{sn}	0.85
Latent heat of fusion of ice	L_{fi}	3.34×10^5 J/m^3
Latent heat of vaporization of water	L_e	2.5×10^9 J/m^3
Latent heat of fusion of snow	L_{fsn}	3.34×10^5 J/m^3
Latent heat of sublimation of snow	L_{ssn}	2.834×10^6 J/m^3
Specific heat capacity of ocean	c_{pa}	3985 J/m^3/°C
Specific heat capacity of air	c_{po}	1004 J/m^3/°C
Density of air	ρ_a	1.3 Kg/m^3
Density of ice	ρ_i	900 Kg/m^3
Density of snow	ρ_s	330 Kg/m^3
Density of ocean	ρ_o	1024 Kg/m^3
Melting point of freshwater ice	t_{fus}	0°C
Salinity of sea ice	s_i	4 psu
Exchange coeff. for sensible heat (leads/ice)	c_H	1.75×10^{-3}
Exchange coeff. for latent heat over leads	c_E	1.75×10^{-3}
Exchange coeff. for latent heat over ice	c_E	1×10^{-3}
Stefan-Boltzmann constant	K	5.67×10^{-8}
Minimum vertical viscosity	υ_{min}	1×10^{-3}

Table 2: Physical parameters of atmosphere, sea ice and ocean.

Experiment	***P**** **(N/m^2)**	**R factor (km)**
CASE 1	*27500*	*25*
CASE 2	*5000*	*25*
CASE 3	*27500*	-
CASE 4	27500	*50*

Table3: Sensitivity tests of sea ice evolution with respect to *P** and R factor.

Experiment	*H* (m)	R factor (km)
CASE 5	0.2	50
CASE 6	0.3	50
CASE 7	0.4	50
CASE 8	f (V)	50
CASE 9	0.2	-

Table 4: Sensitivity tests of sea ice evolution with respect to H and R factor.

Experiment	Sea Ice production (km^3) in July 2000
CASE 5	10.08
CASE 6	11.09
CASE 7	12.12
CASE 8	9.79
CASE 9	6.83

Table 5: Sea ice production in July 2000 for the CASE 5, CASE 6, CASE 7, CASE 8 and CASE 9 experiments.

Table(s)

Click here to download Table(s): Table 6.docx

	Experiment		c_{da}	c_{do}	
1	***E_{15}***	**CTRL**	1×10^{-3}	5×10^{-3}	-
	E_{35}		3×10^{-3}	5×10^{-3}	
	E_{11}		1×10^{-3}	1×10^{-3}	
	E_{31}		3×10^{-3}	1×10^{-3}	
	E_{34}		3×10^{-3}	4×10^{-3}	
	Ec_{da}/c_{do}		1×10^{-3} $V \leq 10$ m/s 3×10^{-3} $V \geq 20$ m/s	$1.3 \times c_{da}$	
2	***Ew_{15}***		$= E_{15}$		Wind Enhancement
	Ew_{31}		$= E_{31}$		
	Ew_{34}		$= E_{34}$		
	$Ew_{cda/cdo}$		$= Ec_{da}/c_{do}$		

Table 6: Sensitivity tests with respect to the air-ice and ice-ocean coefficients.

Winter months	Maximum Polynya extent (km^2)	Mean Polynya extent (km^2)
March	7946	5574
April	1806	1174
May	2688	871.2
June	2205	557.2
July	2962	532.5
August	2868	766.9
September	2674	875.6
October	5637	2304

Table 7: Monthly maximum and mean polynya extent of the TNB polynya.

Winter months	Maximum daily rates of sea ice production (km^3/day)	Mean daily rates of sea ice production (km^3/day)	Monthly cumulative sea ice (km^3)
March	0.42	0.16	4.99
April	0.40	0.26	7.86
May	0.61	0.30	9.25
June	0.54	0.25	7.52
July	0.70	0.22	6.98
August	0.58	0.30	9.39
September	0.44	0.24	7.34
October	0.39	0.14	4.29

Table 8: Daily sea ice production rates from ice production rates spatially cumulated over TNB polynya area.

TNB polynya event in July 2005	Model-derived polynya extent (km^2)	MODIS-derived polynya extent (km^2)
28th 12:00	12	40
29th 06:00	0	25
29th 15:00	389	391
30th 06:00	1858	1936
30th 12:00	2148	2385
31th 03:00	2831	3393

Table 9: TNB polynya extents from model sea ice concentration outputs and from MODIS IST from 28th to 31th July 2005.

Figure(s)

Click here to download high resolution image

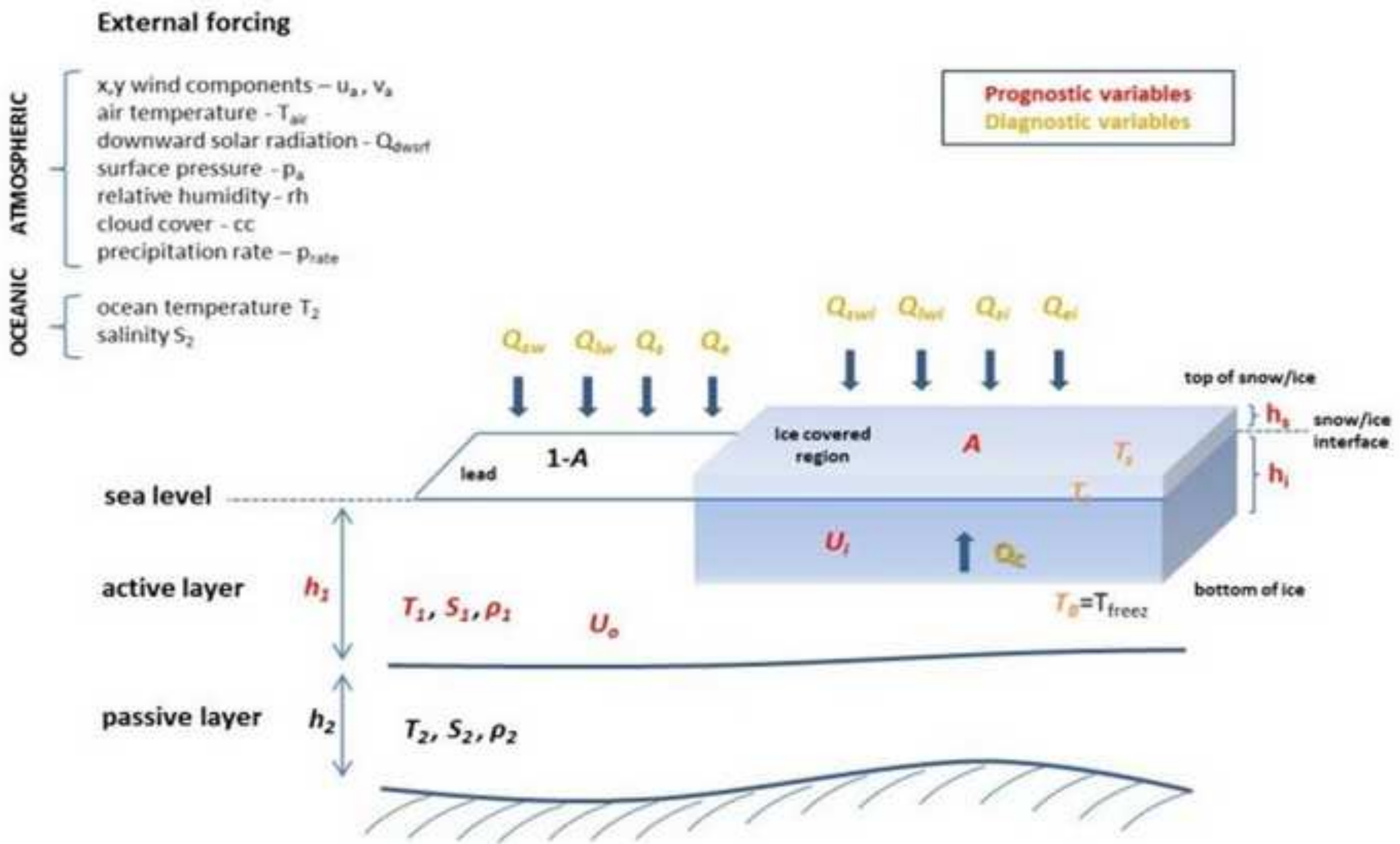

Fig. 1: Schematic view of the main variables of the coupled sea ice – ocean model. The radiative and turbulent heat fluxes (Wm^{-2}) are separately calculated over the ice free (leads) and ice covered part of a grid cell. The positive vertical direction is downward.

Figure(s)

Click here to download high resolution image

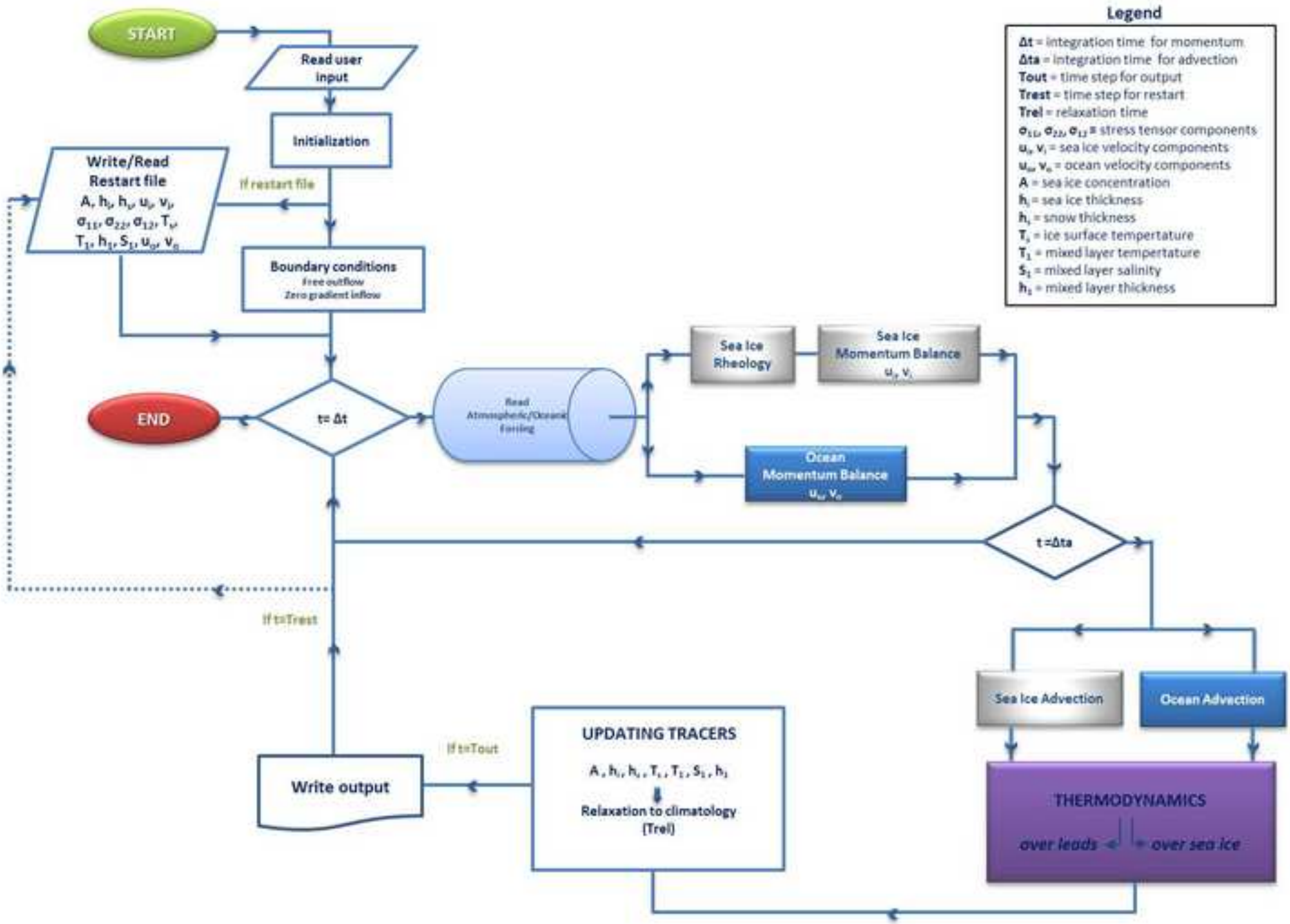

Fig. 2: Diagram flow of the coupled sea ice-ocean model.

Figure(s)
Click here to download high resolution image

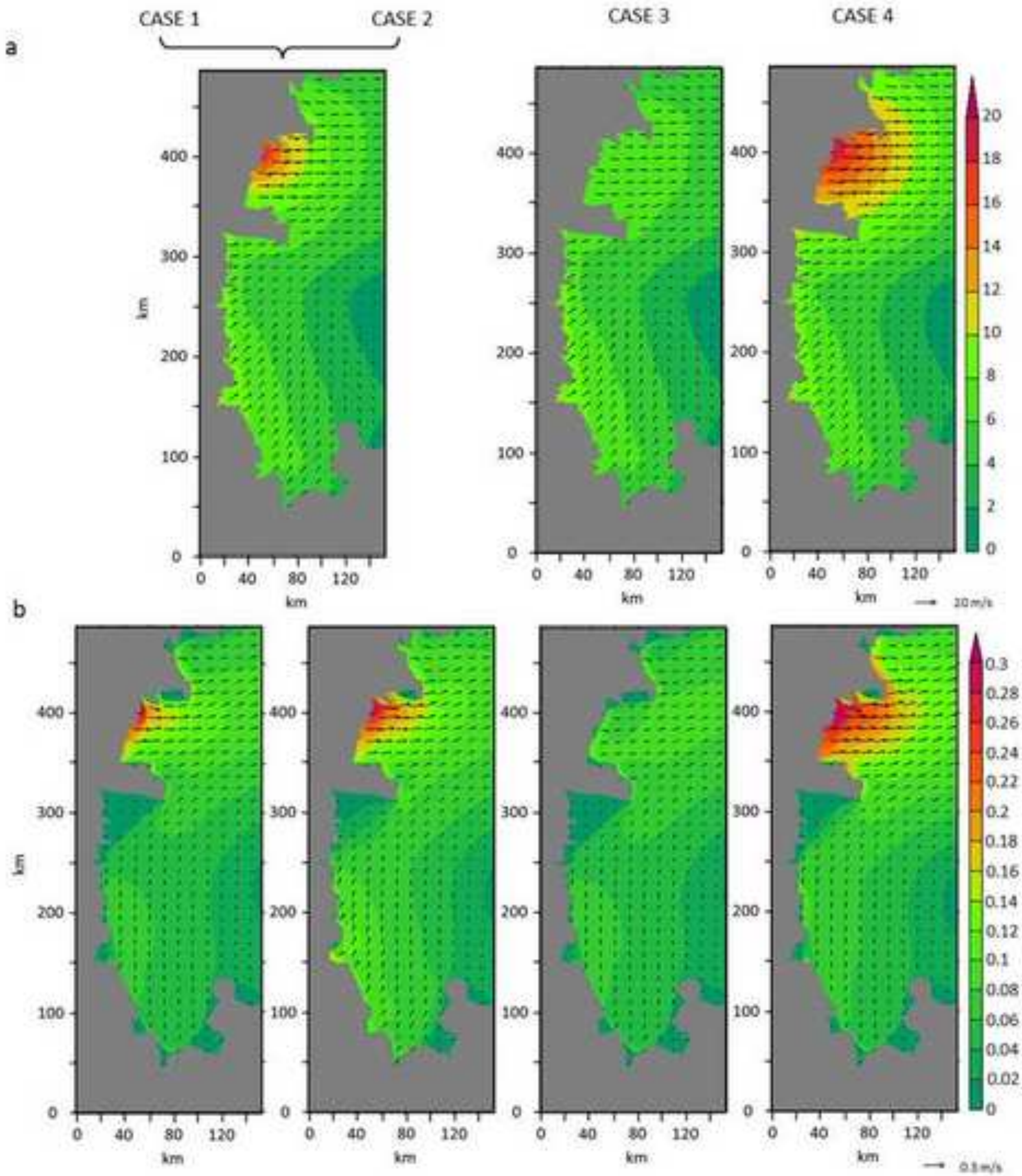

Fig. 3: Maps of wind velocities (a) and modelled ice drift velocities (b) on 8th July 2000 for CASE 1/CASE 2, CASE 3 and CASE 4.

Figure(s)

Click here to download high resolution image

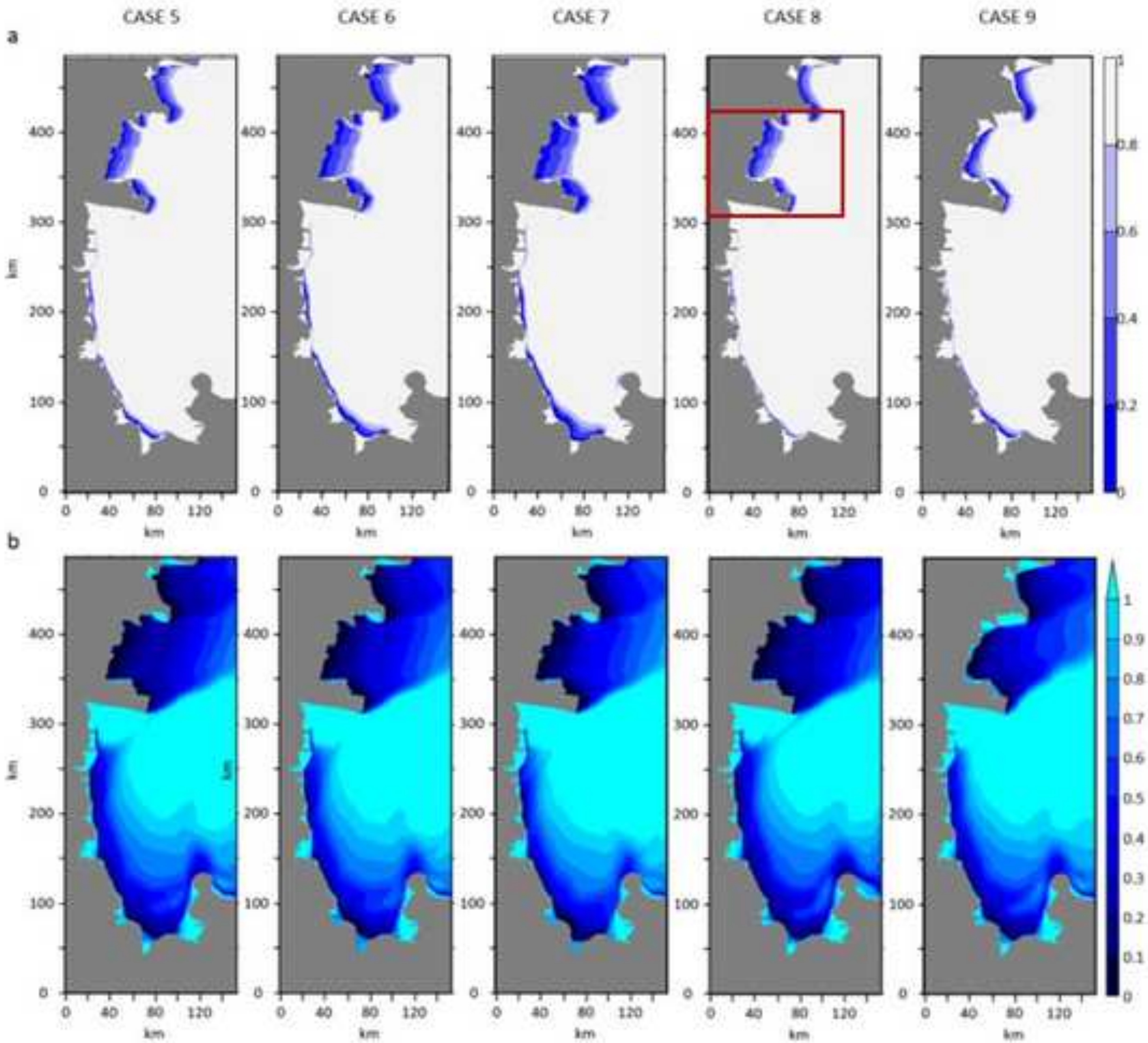

Fig. 4: Simulation maps of sea ice concentration (a) and sea ice thickness (b) for CASE 5, CASE 6, CASE 7, CASE 8 and CASE 9 on 8th July 2000. The portion of the domain marked by the red box in (a) is the area defined for computational purposes as TNB region extending approximately from 310 km to 425 km in Y and bordered by X = 120 km .

Figure(s)
Click here to download high resolution image

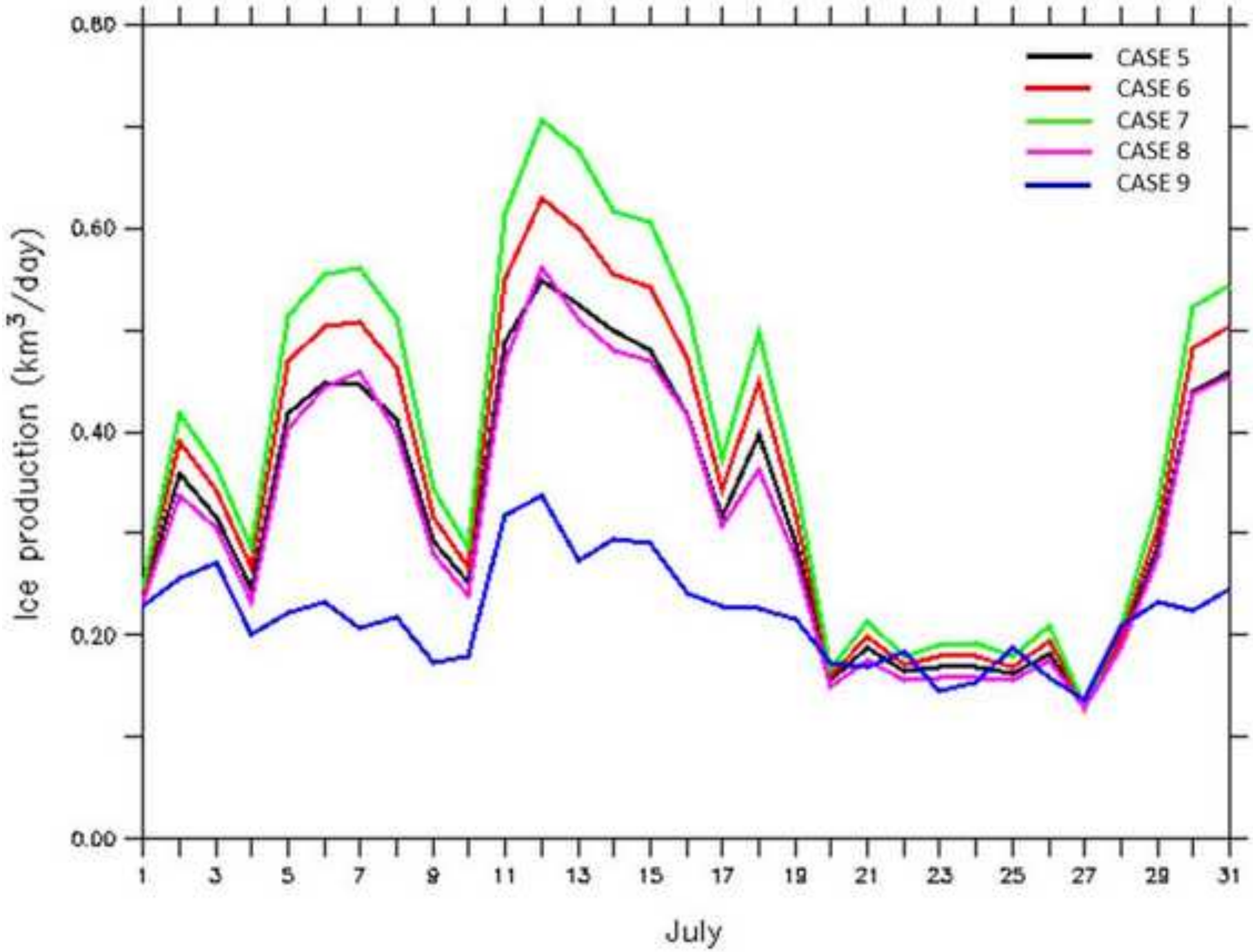

Fig. 5: Daily ice production in the TNB region on 8th July 2000 for CASE 5, CASE 6, CASE 7, CASE 8 and CASE 9 .

Figure(s)

Click here to download high resolution image

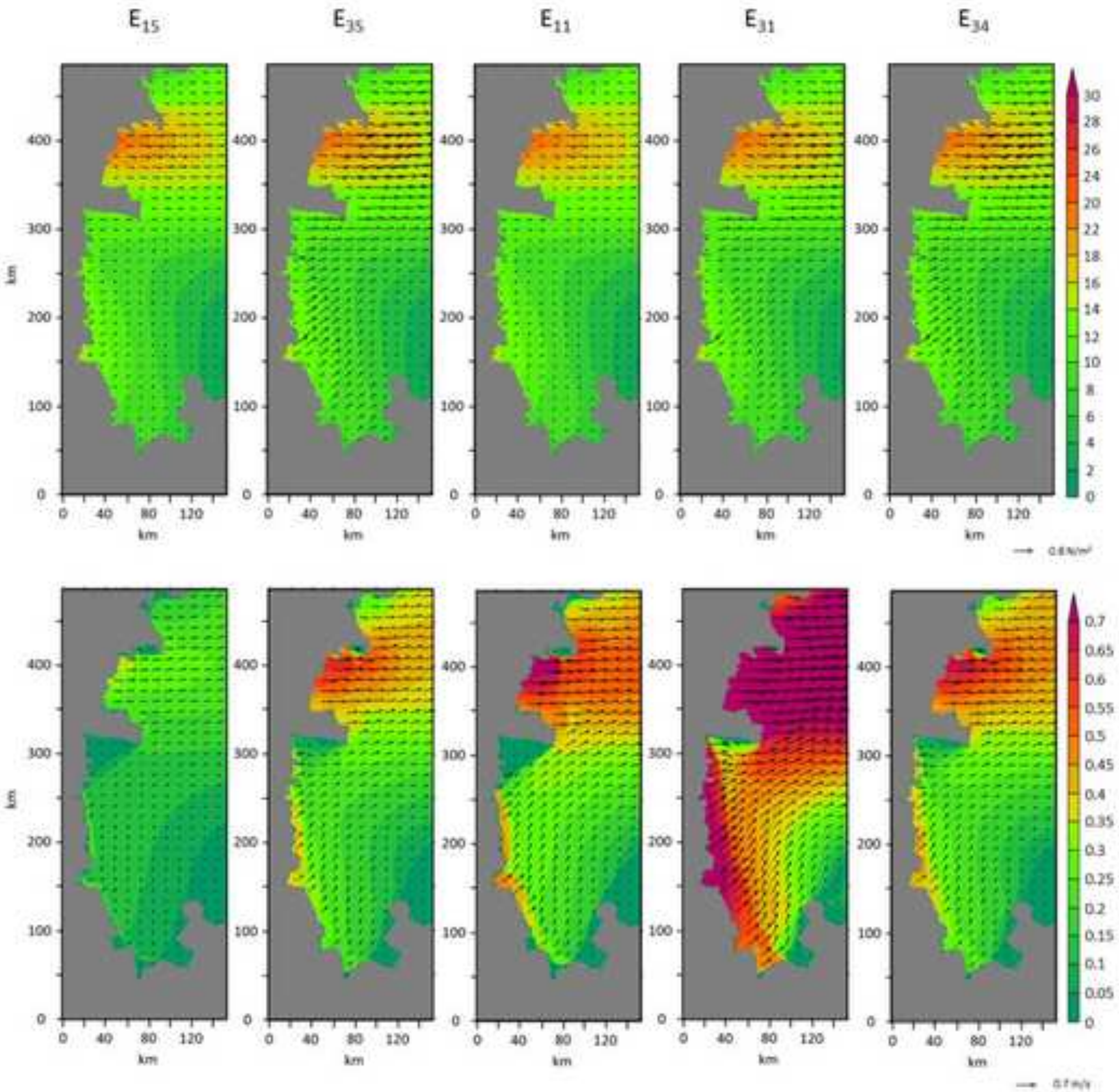

Fig. 6: Wind speed with the superimposed wind stress (on the top) and sea ice drift velocities (on the bottom) on 30th July 2005 for E_{15}, E_{35} E_{11} E_{15} E_{31} E_{34}. The scale arrows on the right indicate the length of the wind stress vector and ice velocity vector, respectively 0.8 N/m^2 and 0.7 m/s.

Figure(s)
Click here to download high resolution image

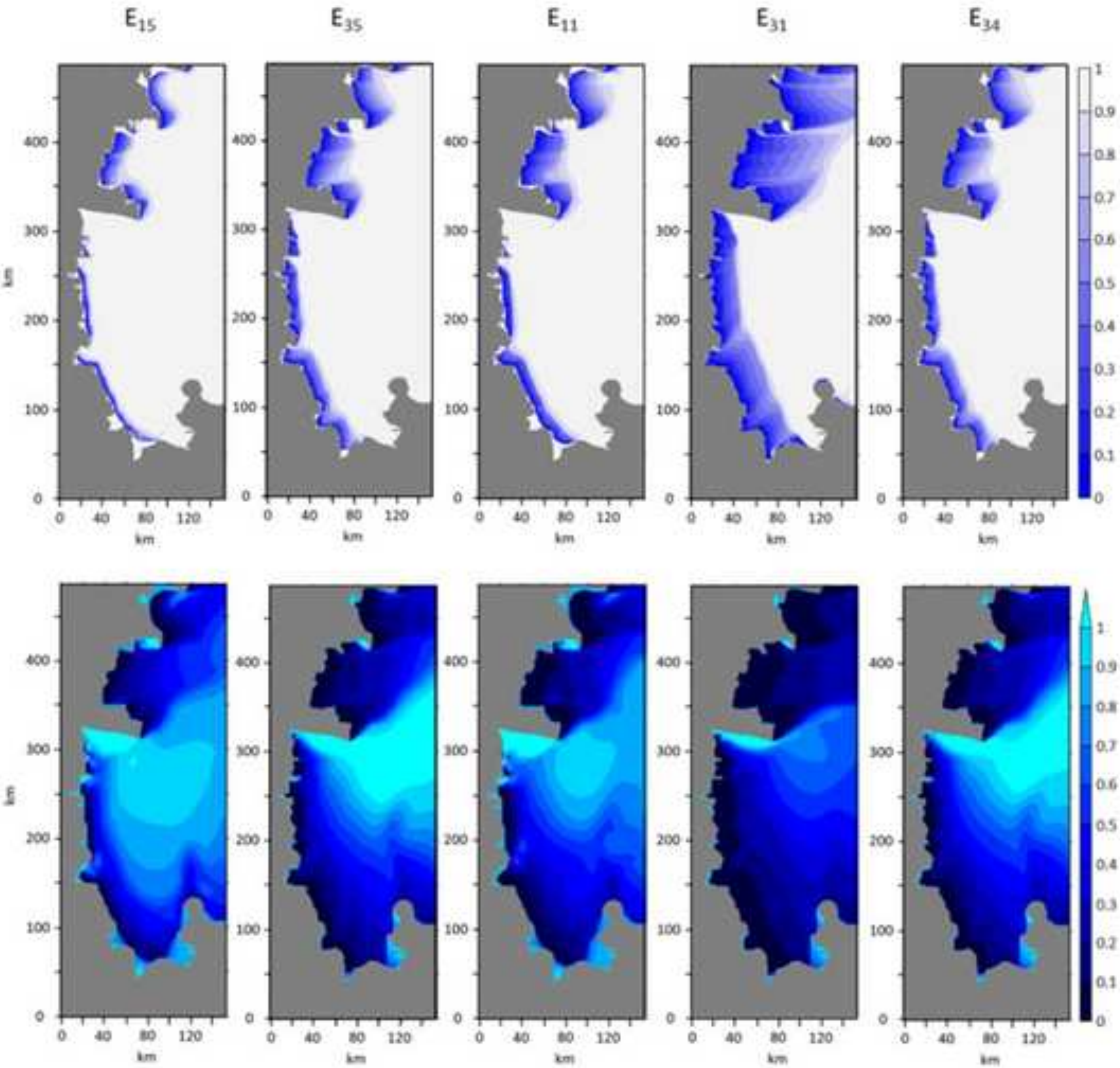

Fig. 7: Sea ice concentration (on the top) and sea ice thickness (on the bottom) on 30th July 2005 for E_{15}, E_{35} E_{11} E_{15} E_{31} E_{34}.

Figure(s)
Click here to download high resolution image

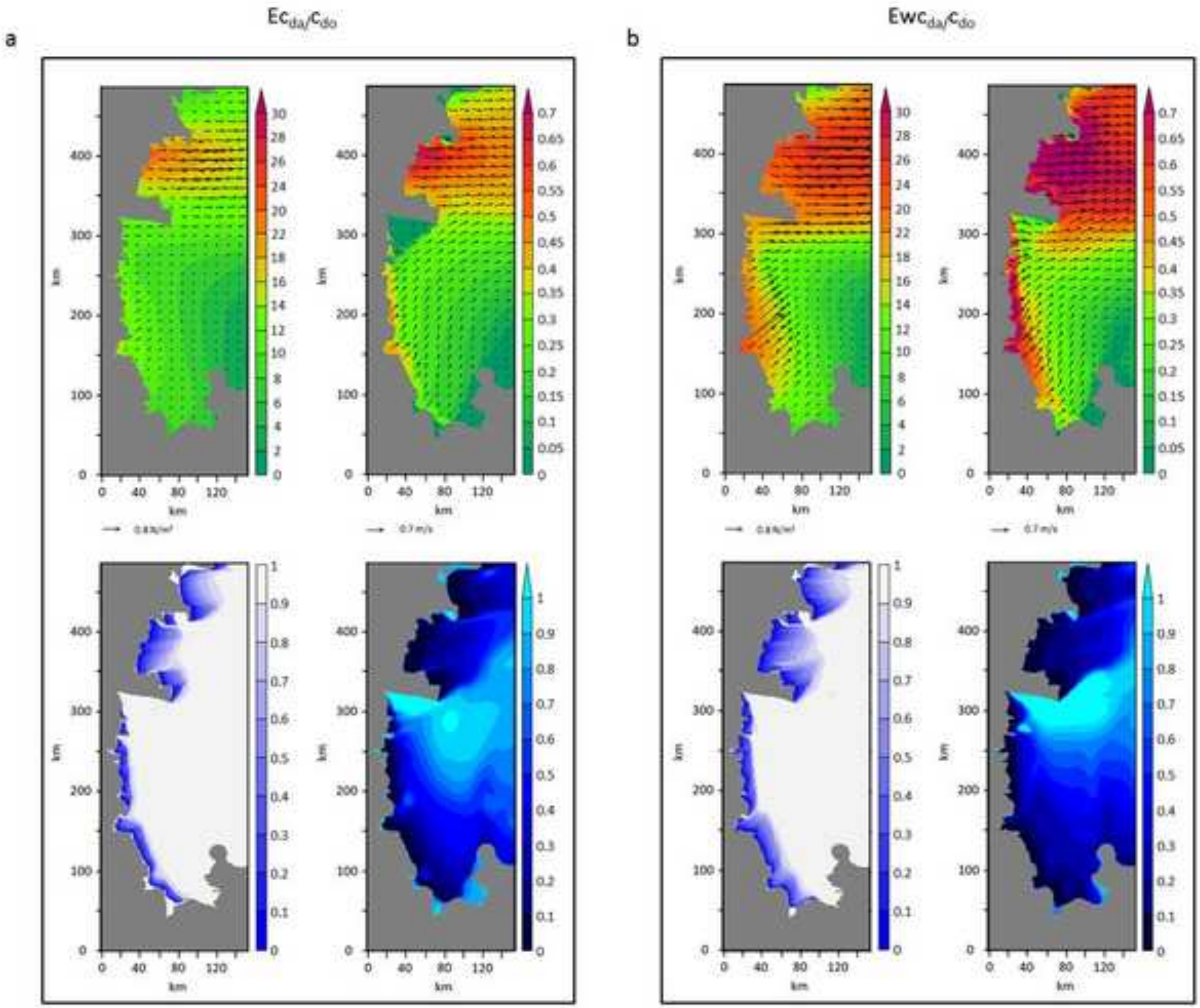

Fig. 8: Wind fields and modelled sea ice drift fields (on the top) and the corresponding sea ice concentration and thickness distribution (on the bottom) on 30th July 2005 for $Ec_{da}c_{do}$ (a) and $Ewc_{da}c_{do}$ (b) run without and with the enhancement function respectively.

Figure(s)
Click here to download high resolution image

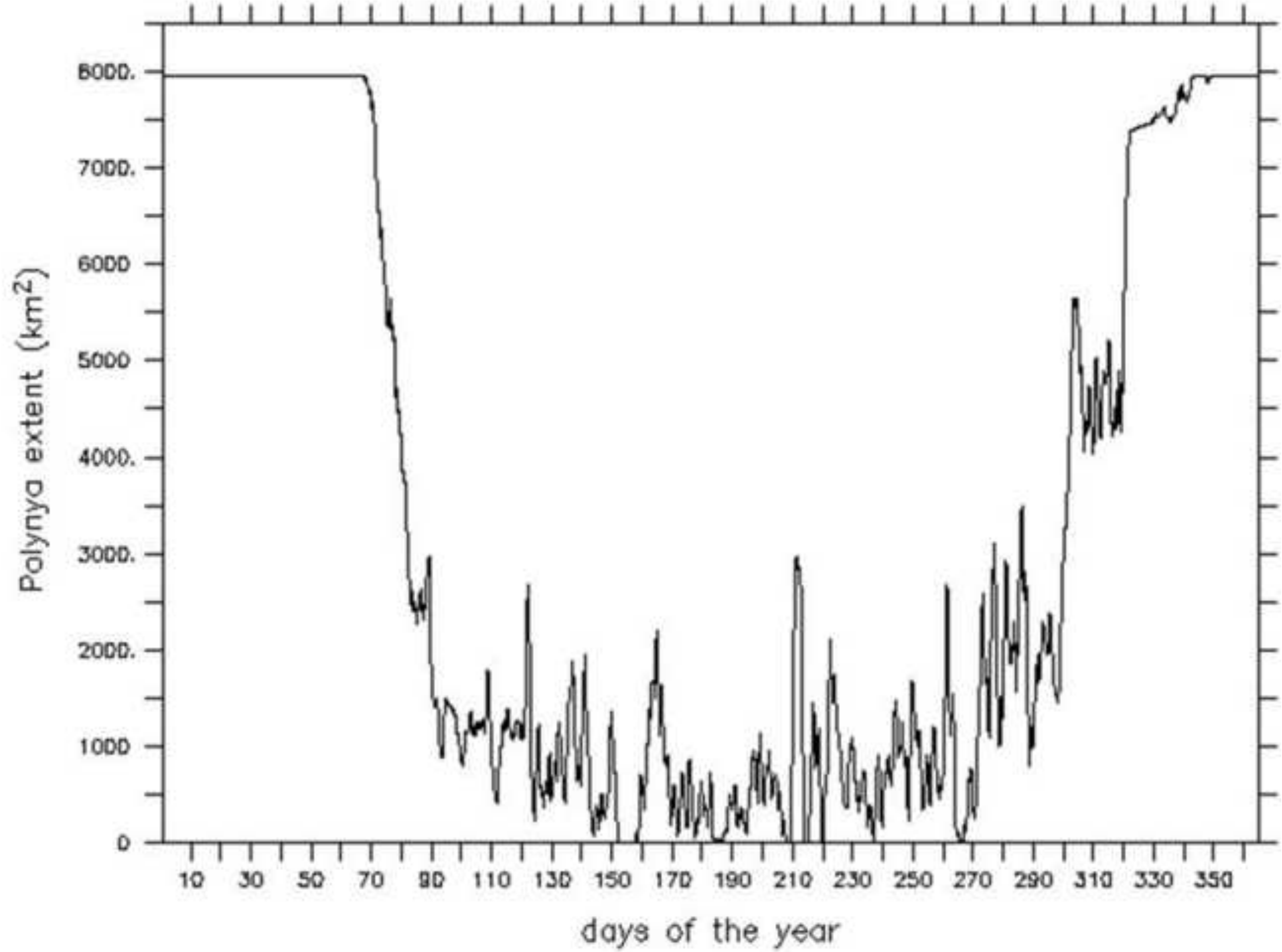

Fig. 9: Model-derived polynya extent in the TNB region in the year 2005.

Figure(s)
Click here to download high resolution image

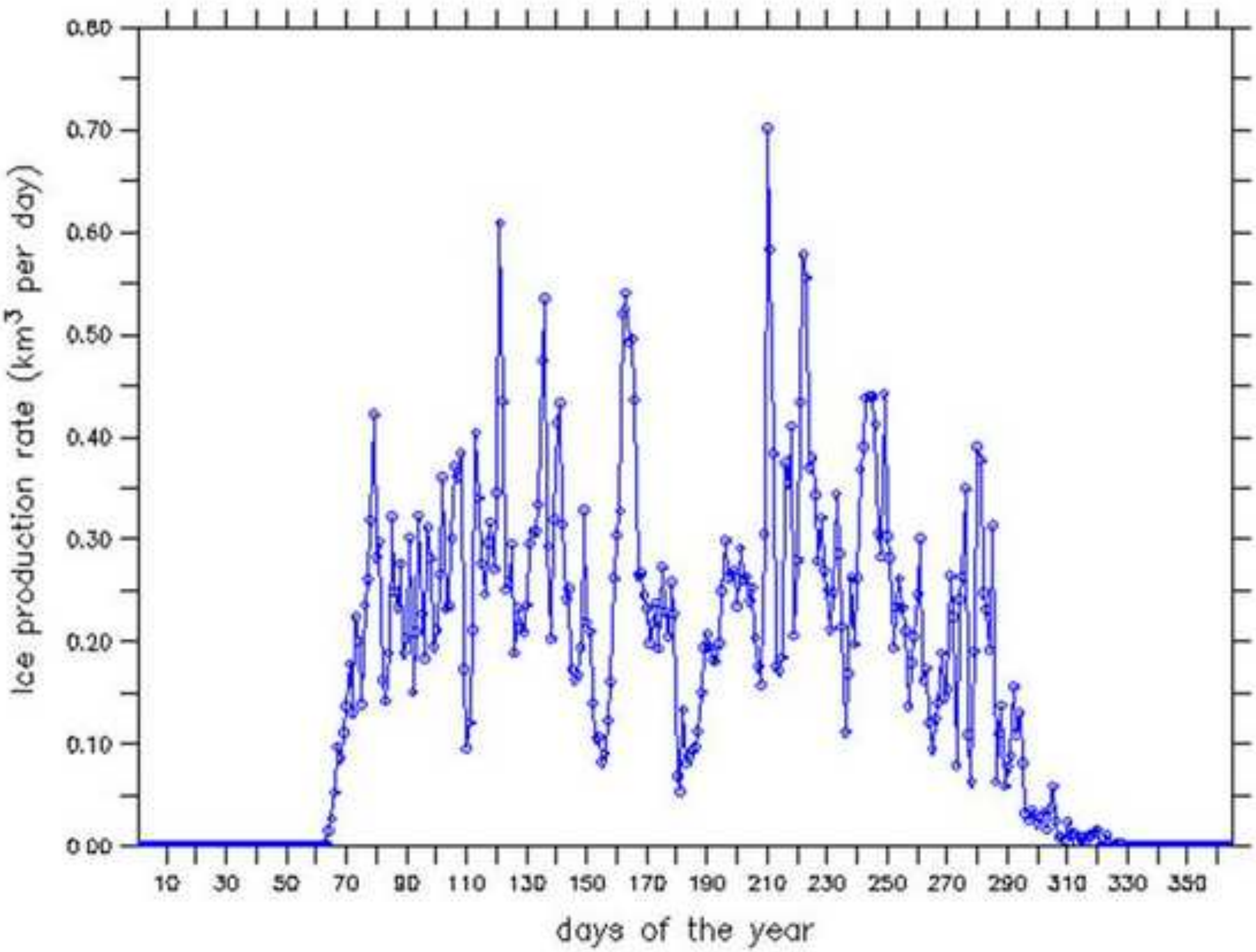

Fig. 10: Spatially cumulated daily rate of sea ice production for the TNB region in the year 2005 .

Figure(s)
Click here to download high resolution image

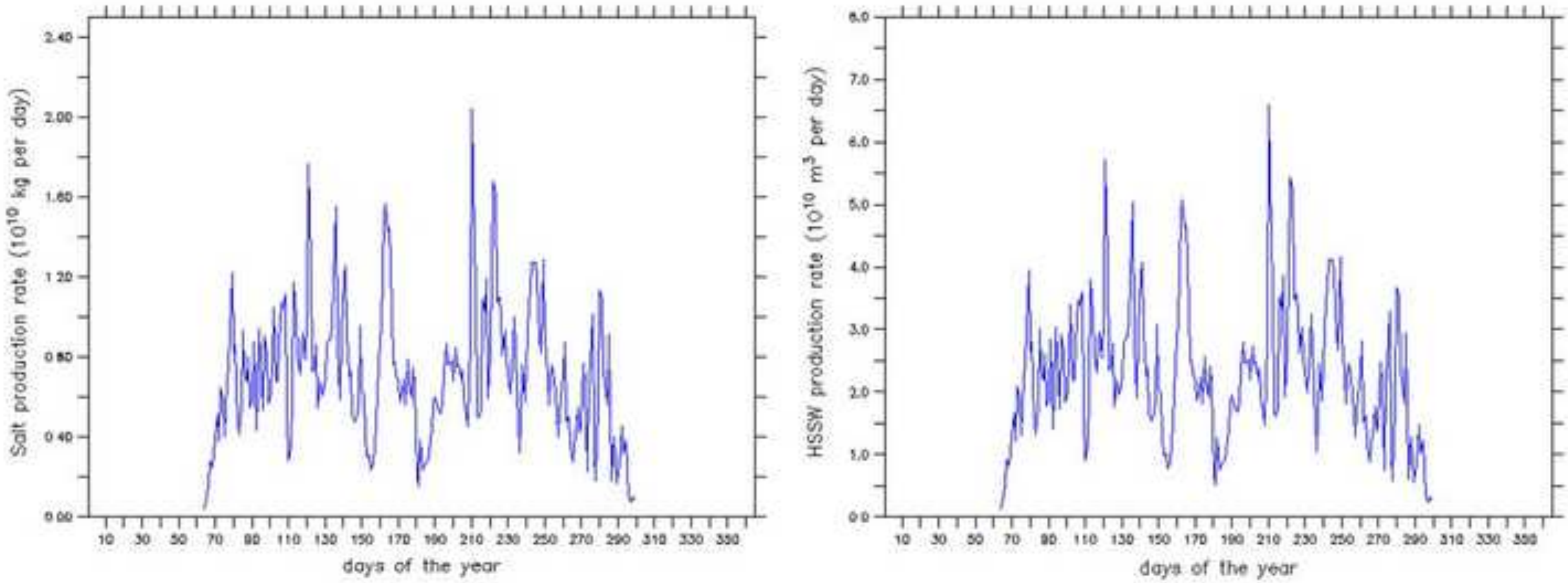

Fig. 11: Salt production rate (on the left) and HWSS production rate (on the right) in the TNB polynya area in the year 2005.

Figure(s)
Click here to download high resolution image

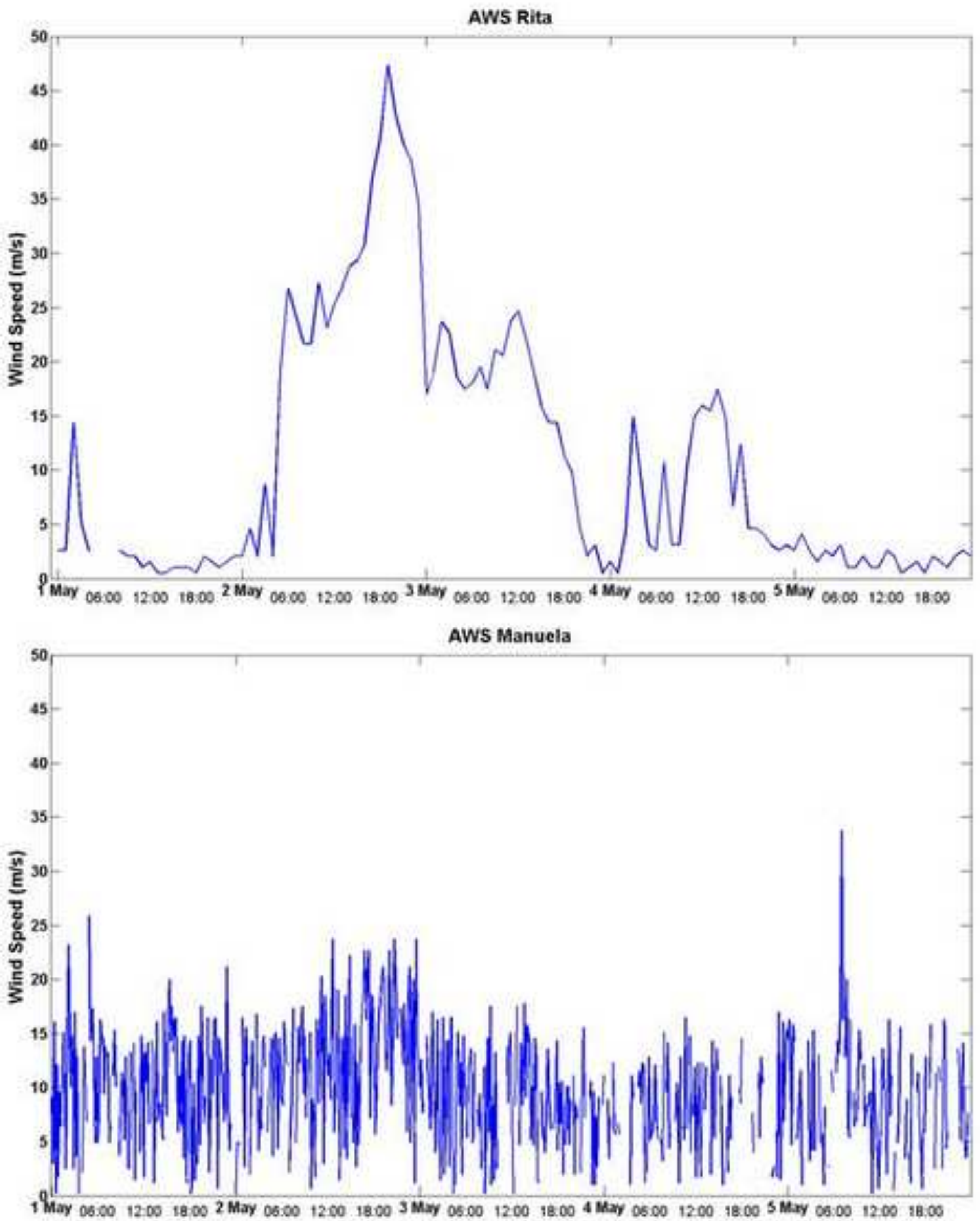

Fig. 12: Wind speed from Rita (on the top) and Manuela (on the bottom) AWSs on 1-5th May 2005.

Figure(s)
Click here to download high resolution image

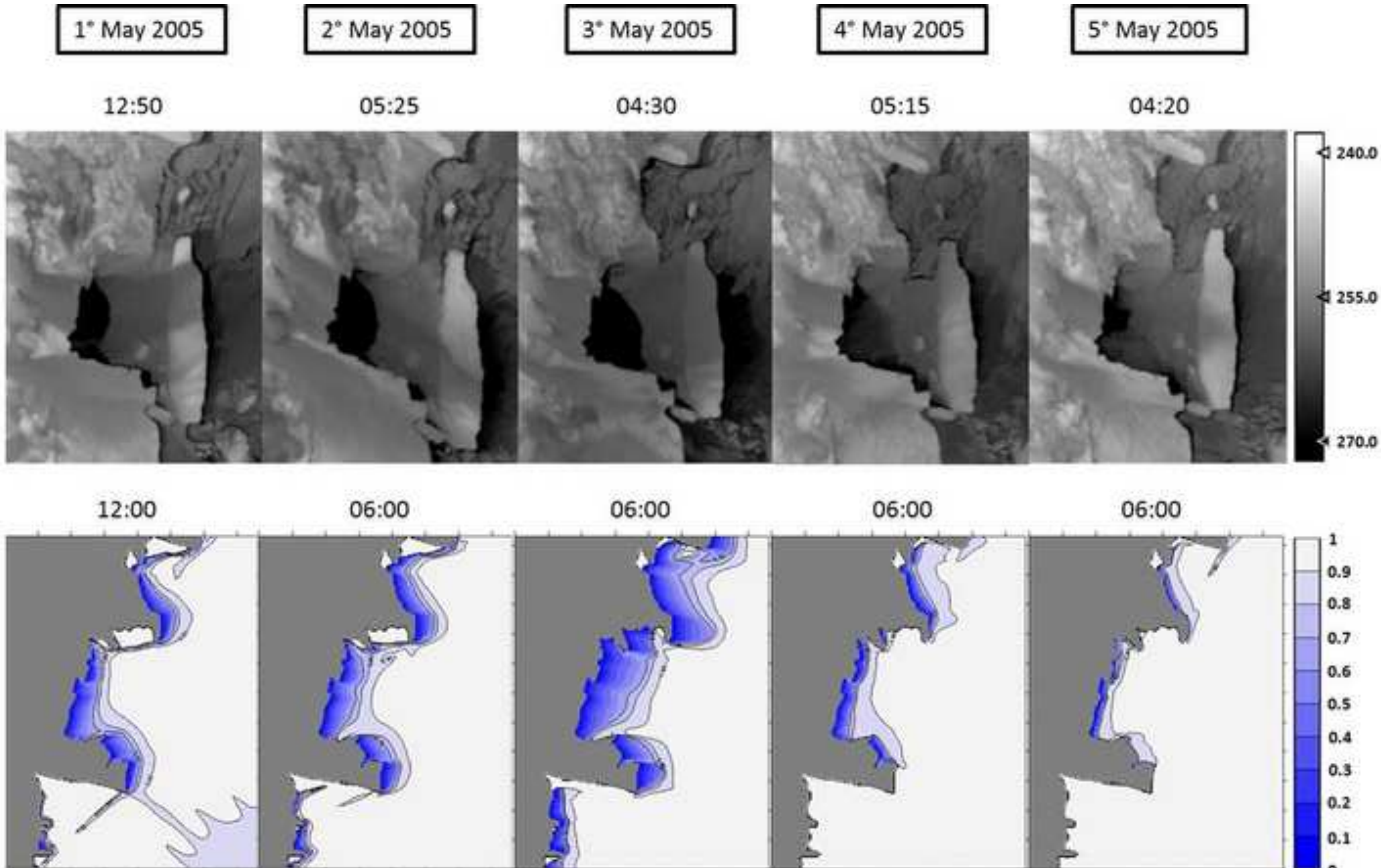

Fig. 13: IST MODIS scenes (on the top) and the modelled sea ice concentration maps (on the bottom) displaying the polynya evolution on 1-5th May 2005.

Figure(s)
Click here to download high resolution image

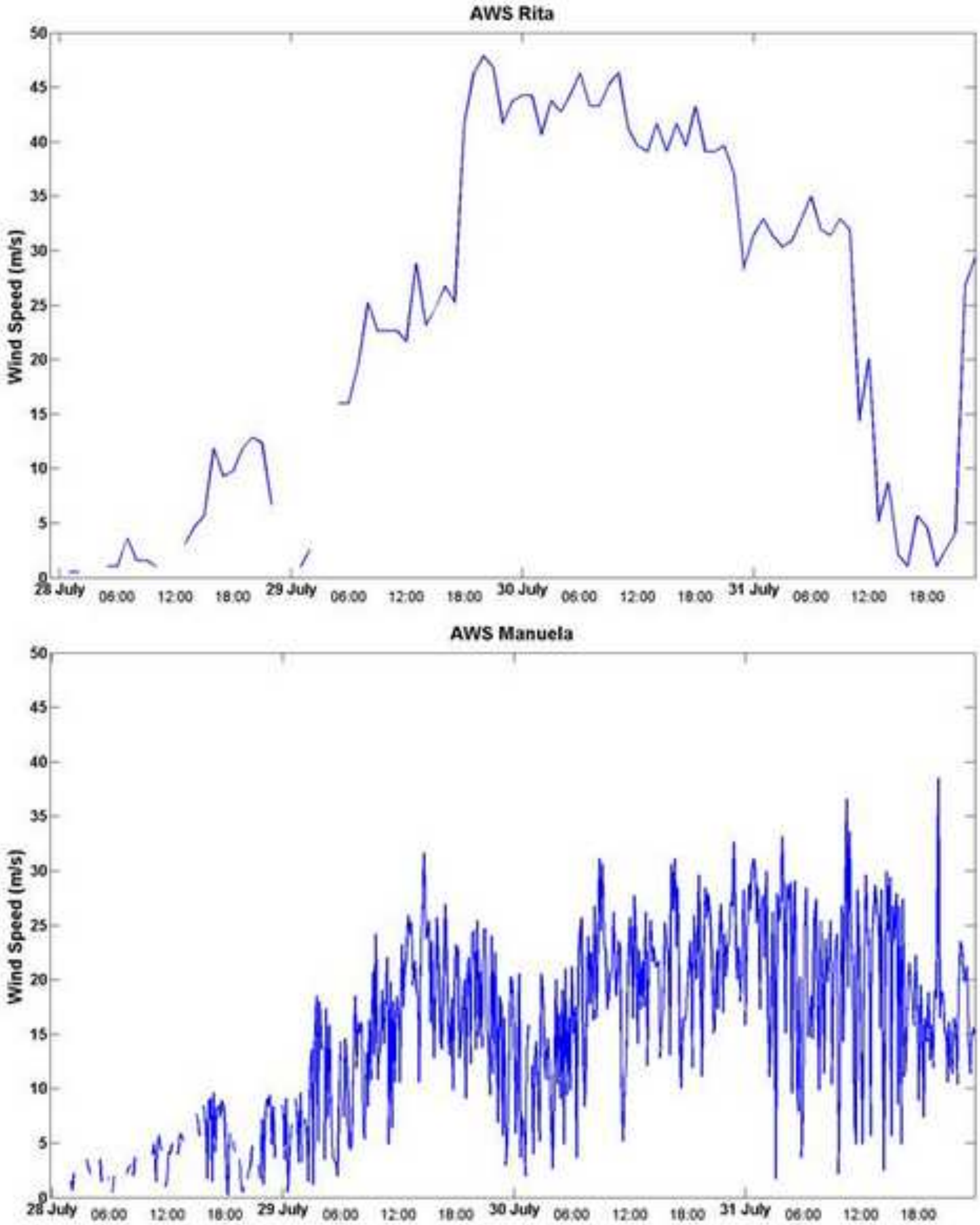

Fig. 14: Wind speed from Rita (on the top) and Manuela (on the bottom) AWSs on 23-31th July 2005.

Figure(s)

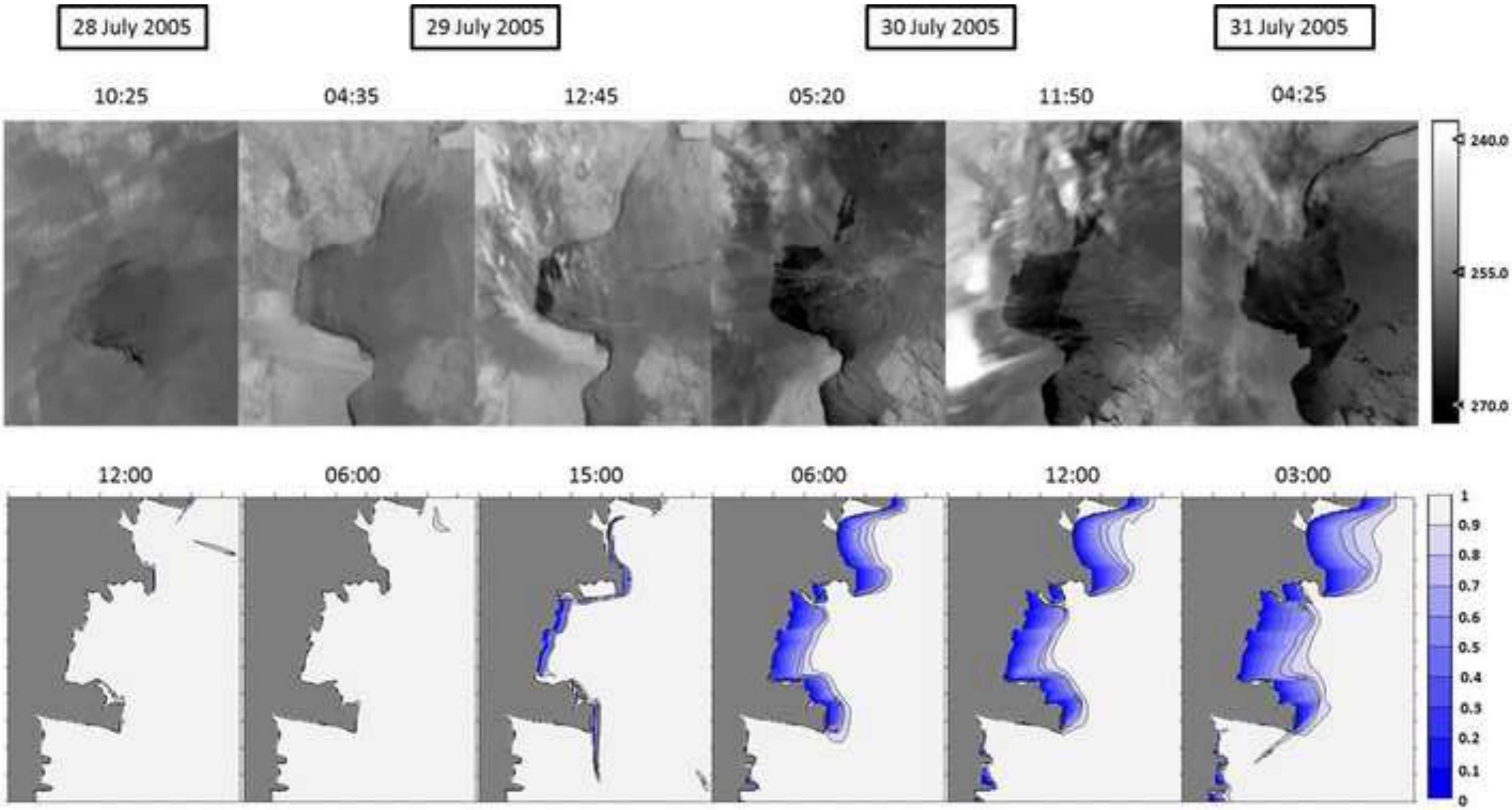

Fig. 15: IST MODIS scenes (on the top) and the modelled sea ice concentration maps (on the bottom) displaying the polynya evolution on 23-27th July 2005.